Order Number 1350788

Intersymbol interference characterization and equalization for high density optical data storage

Gupta, Sunil, M.S.

The University of Arizona, 1992

U·M·I
300 N. Zeeb Rd.
Ann Arbor, MI 48106

INTERSYMBOL INTERFERENCE CHARACTERIZATION AND EQUALIZATION FOR HIGH DENSITY OPTICAL DATA STORAGE

by

Sunil Gupta

A Thesis Submitted to the Faculty of the

DEPARTMENT OF ELECTRICAL AND COMPUTER ENGINEERING

In Partial Fulfilment of the Requirements

For the Degree of

MASTER OF SCIENCE

WITH A MAJOR IN ELECTRICAL ENGINEERING

In the Graduate College

THE UNIVERSITY OF ARIZONA

1992

STATEMENT BY AUTHOR

This thesis has been submitted in partial fulfilment of requirements for an advanced degree at The University of Arizona and is deposited in the University Library to be made available to borrowers under rules of the library.

Brief quotations from this thesis are allowable without special permission, provided that accurate acknowledgment of the source is made. Requests for permission for extended quotation from or reproduction of thesis manuscript in whole or in part may be granted by the head of the major department or the Dean of the Graduate College when in his or her judgment the proposed use of the material is in the interests of scholarship. In all other instances, however, permission must be obtained from the author.

SIGNED: Sunil Gupta

APPROVAL BY THESIS DIRECTOR

This thesis has been approved on the date shown below:

Ming-Kang Liu
Assistant Professor of
Electrical and Computer Engineering

9/28/92
Date

ACKNOWLEDGMENTS

I wish to gratefully acknowledge my indebtedness to all individuals who have contributed to both the content and quality of this thesis. It is hard for me to imagine how this work could have been completed without feedback from the faculty members of the Department of Electrical and Computer Engineering. I have been especially fortunate in this regard by having the opportunity to learn from my advisor, Dr. Max M.-K. Liu, and benefit from his constant encouragement and guidance. Also, I would like to thank my thesis committee members, Dr. Masud Mansuripur and Dr. Michael W. Marcellin, for reviewing this thesis.

Finally appreciations are due to my friends, Mr. Mariappan S. Nadar, Mr. Babak Tehranchi and Mr. Sriram Parthasarathy for their support throughtout my Masters program.

TABLE OF CONTENTS

LIST OF FIGURES

ABSTRACT

In optical data storage, intersymbol interference (ISI) is one of the limiting factors for high storage density. To reduce ISI, we need to understand its characteristics and use appropriate signal processing techniques. In this thesis, we characterize ISI for various data patterns and compare Signal to Noise Ratios (SNR) with and without ISI equalization. To characterize ISI, we sample the readback waveforms and use a computer program for data processing. To compare SNR with and without equalization, we record a pseudo random sequence and compare the detected marks with original marks. We also compute SNR using the additive interleaving detection (AID) technique without ISI equalization. From our studies, ISI is found to be more significant as mark widths become smaller. We also found that SNR can be increased by 3 to 9 db with equalization. More interestingly, we found that AID gives good SNR even without ISI equalization. This indicates the simplicity of using AID for higher storage density.

CHAPTER 1

Introduction

Optical data storage has become important for its high storage density, random access, rewritability, portability, and long archival life. An areal storage density of 0.5×10^6 bits/mm^2 has been reported [3]. In addition to the high density, the ability to read and write small bits with a large mechanical clearance leads to many favorable attributes in optical storage. It enables second-surface operation, which greatly improves immunity to surface dirt and scratches, and allows good isolation of the active film from the atmosphere. This in turn permits the removal of media, consequently enabling the drive to be used with any medium (erasable, non-erasable and read only). This disk portability requires no extra servo requirement because of the stricter requirement for high density tracking. Furthermore, because of this mechanical clearance, we can have longer archival life and there is no possibility of head "crashes" that destroy stored data. Therefore, optical drives can have lesser shock and vibration control as compared to magnetic storage.

1.1 Issues in Optical Data Storage and Thesis Objective

Although optical data storage has large storage densities, it has longer access time and lower transfer rates than magnetic storage. Longer access time is due to heavier laser heads, and lower transfer rates are due to limited laser power. Furthermore, not every optical storage system is rewritable. M-O and phase change [3] systems have been developed in the past for rewritability. However, in these systems, writing data takes two cycles: one cycle to erase and one cycle to write. Therefore, this is more time consuming than magnetic storage.

In this thesis, we will study techniques to increase the storage density for Magneto-Optic Systems. Although smaller spot-size recording using short wavelength laser diodes is one important approach, to fully take advantage of this shorter wavelength recording, we need to carefully control the other two important factors: intersymbol interference (ISI) and pulse broadening.

Pulse broadening (can be actually shrinking) is the change of the pulse width when it is written and read back again from the original. When a sequence of marks is written to a disk, the real size of each mark is not determined by itself but also by adjacent marks. When marks are read, each pulse width is also subject to itself and neighboring marks. This change in pulse due to neighboring marks is called ISI. When the neighboring marks have large widths, the ISI effect is not important because the central mark is more like an isolated mark. However, when mark widths become smaller as we use shorter wavelengths, this ISI effect becomes important and a careful ISI equalization is necessary.

From the discussion, the objective of this thesis is to quantify the characteristics of intersymbol interference (ISI) and pulse broadening experimentally and to evaluate how much signal to noise ratio can be improved. In other words, we want to first get the ISI characteristics and use them for equalization. We will evaluate how this ISI equalization can increase the noise margin in detection.

1.2 Organization of Thesis

In the remainder of the thesis, Chapter 2 first reviews the basic read/write principles of an optical data storage system, and explains coding, modulation and detection schemes for recording. Chapter 3 describes the experimental setup and different data patterns used. Chapter 4 describes the signal processing techniques applied and the characteristics of ISI. Chapter 5 focuses on SNR computation with and without equalization, and finally Chapter 6 gives the discussion from the experimental results with suggestions for future work.

CHAPTER 2

Principles of Optical Data Storage and Pulse Width Modulation

To serve as the background for the following chapters on ISI characterizations and signal processing, this chapter reviews important principles of optical storage systems. Specifically, we explain the read/write principles of magneto-optical storage systems and pulse width modulation (PWM).

2.1 Configuration of Optical Recording System

The basic configuration of a typical magneto-optical (M-O) recording system is shown in Fig. 2.1 [3]. The system consists of a laser diode, two photodetectors, and optical components including polarizing beam splitters and lenses. The M-O disk used has a pre-grooved substrate and is coated with a ferro-magnetic thin film layer consisting of Tb-Fe-Co alloy. This magnetic layer is polarized vertically (up or down) and used for recording 0's and 1's. See Fig. 2.2. To control the polarization or record data, an electromagnet is placed on the disk to supply magnetic field at the recording point.

The first polarizing beam splitter polarizes the light from the laser and focuses it on the disk where it is used for writing and sensing the polarization when reading. When the

polarized light that goes to the disk is reflected, it goes back to the first beam splitter and is reflected to the second beam splitter. This second polarizing beam splitter is rotated 45 degrees about the optical axis so that the incident light is split between the two photodiodes. The detected signals from the photodiodes are used to sense the magnetic polarizations and to provide servo control for laser beam focusing and tracking to maintain the laser spot in precise position relative to the disk surface and data tracks.

2.2 Principles of Magneto-Optical Reading and Writing

This section explains in more detail how data can be recorded and read back. The write and read processes are illustrated in Fig. 2.2. To record data, the recording M-O layer is first polarized uniformly in the same direction before recording. To change the polarization say from up to down, the electromagnet head is supplied a different direction current for opposite magnetization direction. However, if there is no laser beam on the same spot, the polarization cannot be changed because the Curie temperature of the medium is higher than the room temperature. When the focused laser spot irradiates and heats the recording layer up to the Curie temperature, the initial magnetization of the recording layer is changed from up to down at the recorded domain. Erasure of the recorded domain can be done simply by repeating the same process with up magnetic polarization.

To read back the recorded data in the read process, we must be able to detect the polarizations in the medium. To do this, the Kerr effect is used [3], which can be understood as follows. When a linearly polarized laser beam irradiates the recording layer (small enough

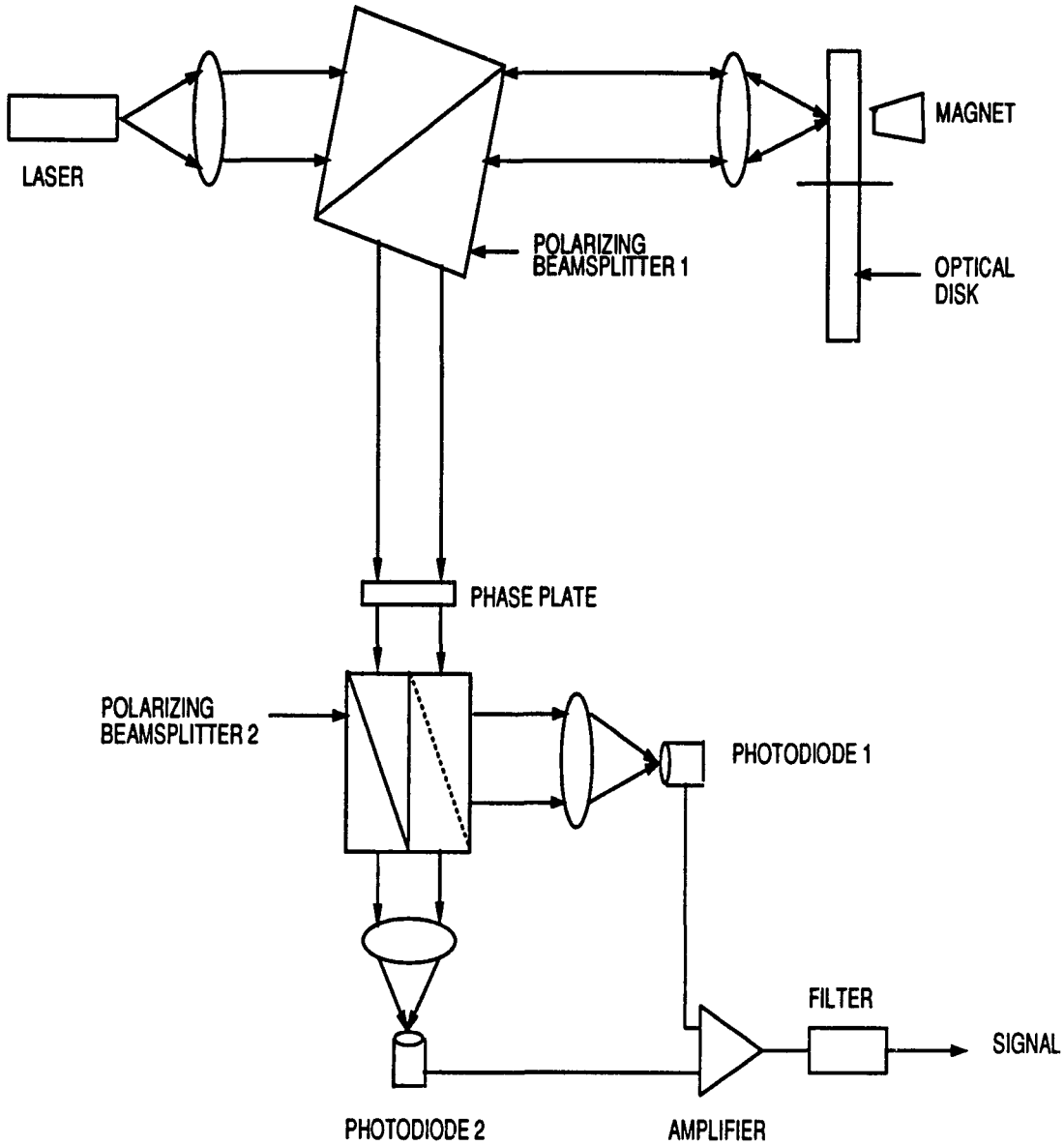

Figure 2.1: Schematic layout of an Optical Data Storage System.

power to avoid changing the polarizations), the polarization of the reflection beam will be determined by the polarization of the irradiated spot. The change in reflected beam polarization angle with respect to incident beam is termed as Kerr rotation. See Fig. 2.2. This rotation is detected by the photodetectors.

From the explanation of the read/write principles, we see that optical recording is done through modulating the magnetic polarization of the recording layer. That is, information bits are stored through modulating marks alternating in polarization or state. In the next section, we will explain how to translate bits into alternating marks and vice versa.

2.3 Pulse Width Modulation, Coding and Detection

In PWM, information bits are stored by modulating mark widths recorded on disks. Modulation codes are used to translate bits into mark widths. One important modulation code is called Run-length-limited (RLL) [3] [1]. Basically, RLL codes introduce additional constraints in the bit sequence before bits are differentially encoded. There are two constraints in RLL codes, denoted by (d,k). The d and k constraints specify that there are at least d and no more than k consecutive zeros between two ones at the output of the RLL encoder. Therefore, alternative marks using differential coding will have width at least (d+1) and not greater than (k+1). The k constraint guarantees enough transitions for bit timing recovery in reading. The d constraint determines the minimum mark size at a given bit length. Therefore, at a given diffraction limit or minimum beam spot that can be achieved, the larger the d, the more encoded RLL bits can be recorded within the minimum mark. This will improve the recording density as long as the RLL

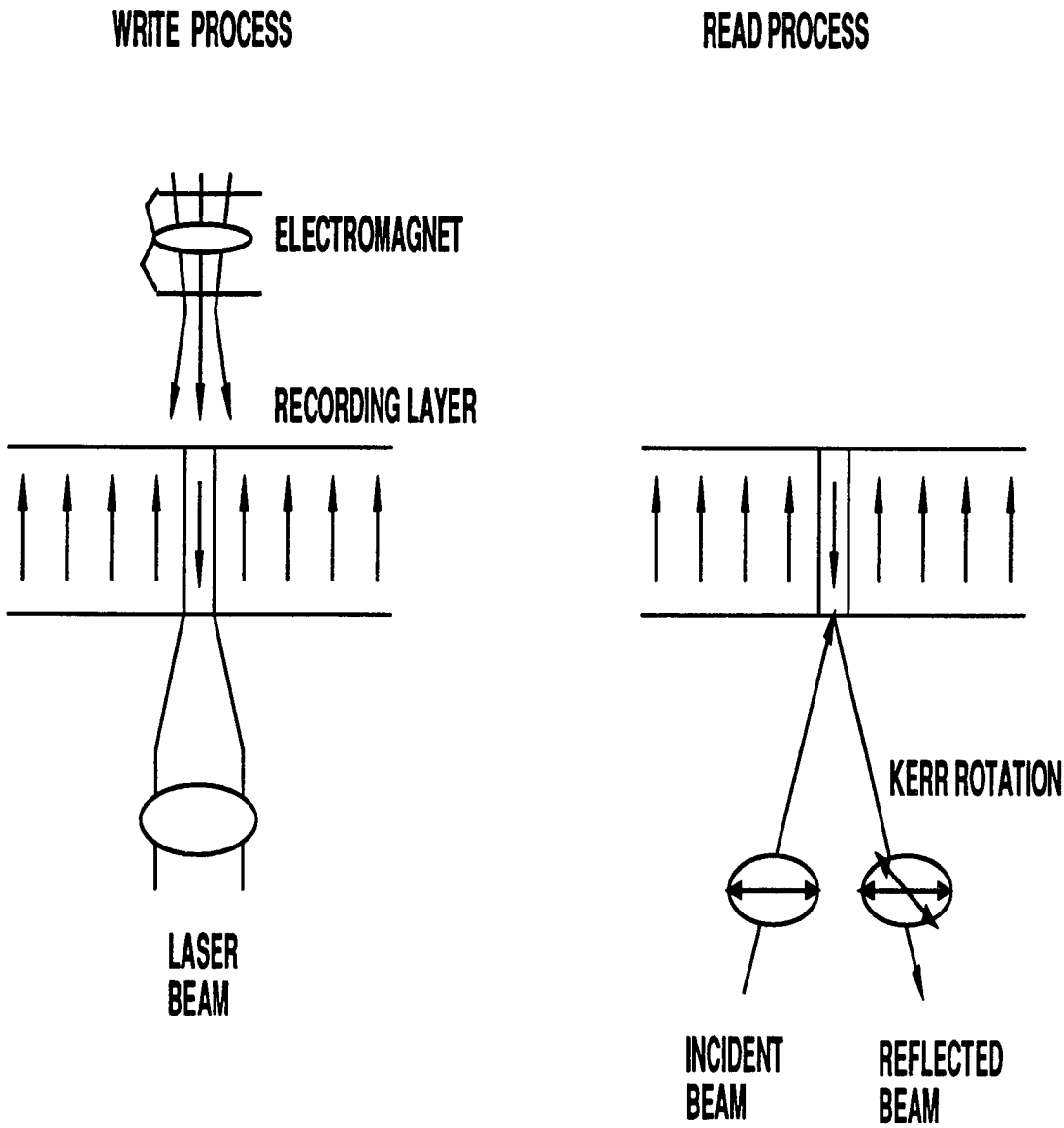

Figure 2.2: Write/Read Mechanism in Optical Data Storage System.

encoding efficiency is not too small to offset the gain from the d factor. The RLL encoding inefficiency is from the fact that when m data bits are encoded into n bits, we have $n > m$. The coding efficiency is the expectation of m/n.

As an example, one very popular RLL code is the (2,7) code. Therefore the minimum mark consists of 3 encoded bits. The coding efficiency of the (2,7) code is found to be 0.5 [3]. Therefore, the storage density can be improved by 50% (3×0.5). The (2,7) code is illustrated in Fig. 2.3. The input data bits, encoded RLL bits, alternative polarization marks, and the readback signal are shown as a function of time.

To recover the recorded bits, we need to detect the width of each mark from the readback signal. A popular method used (although may not be the best) is known as the peak detection technique. In this method, the readback signal is differentiated to generate peaks at the mark boundaries. By locating the peaks or positions of the mark boundaries, mark widths can be determined. Specifically, a bit timing is regenerated from a phase lock loop (PLL) in the detection circuitry. From the bit timing recovered, time windows can be defined as the time intervals between clock transitions. Therefore, we can locate mark boundaries by determining which window peaks fall into. More sophisticated detection can by done using the maximum likelihood (ML) and Viterbi algorithm [4] [19].

The readback signal is subjected to a number of degradations which cause detection errors. In addition to noise and material defects, as mentioned earlier in Chapter 1, important sources of degradation include intersymbol interference (ISI) and pulse broadening. In the remaining thesis, we will quantify these degradation sources and use equalization to improve the detection performance.

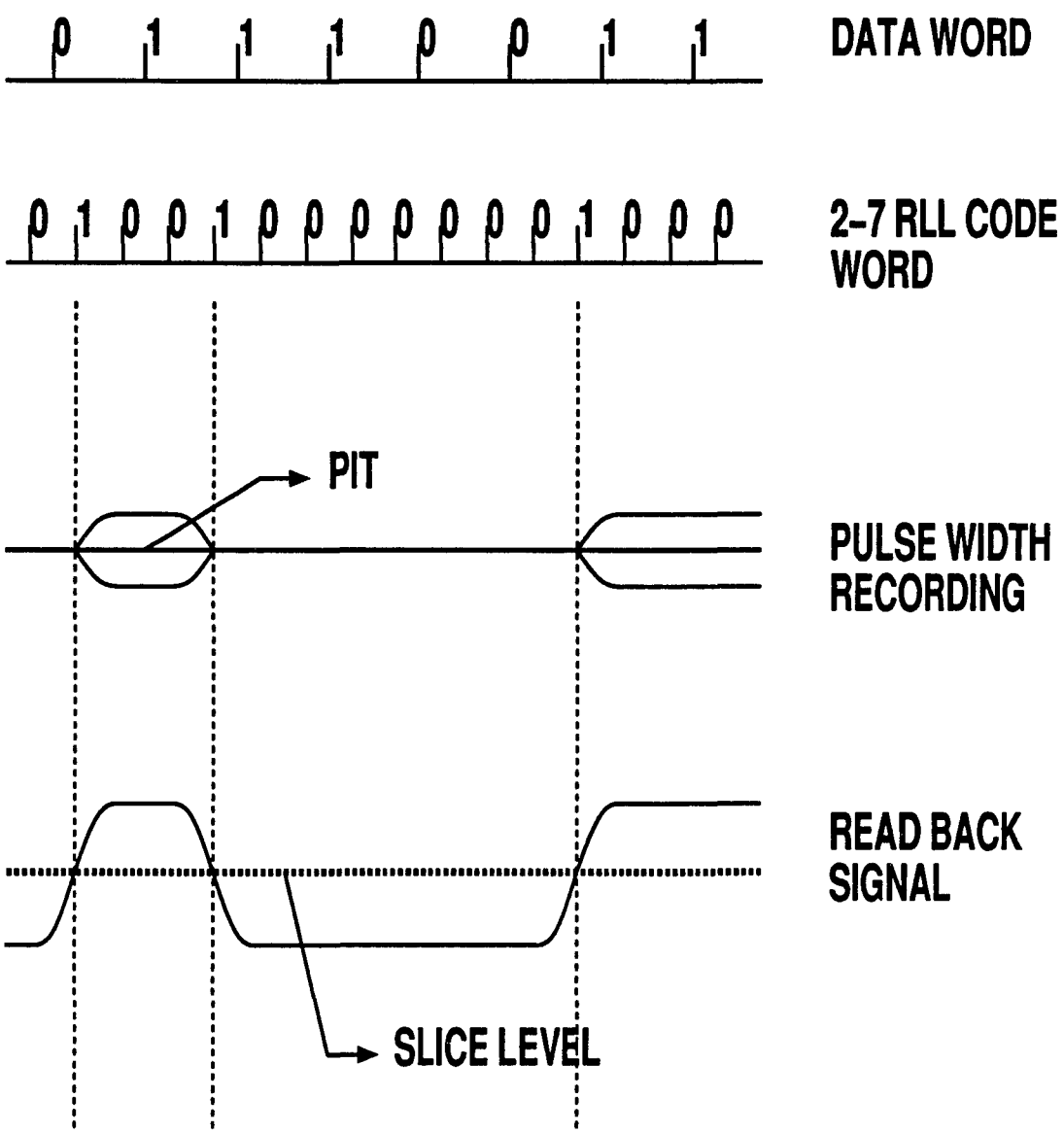

Figure 2.3: Principle of Pulse Width Recording.

CHAPTER 3

Data Acquisition

In this chapter, we describe the experimental setup and various data patterns recorded for ISI characterization.

3.1 Experimental Setup

The block diagram of the experimental setup is depicted in Fig. 3.1. In the setup, a personal computer is used for data pattern generation and acquisition. The data pattern can be arbitrary (up to 2^{31} bits) and is stored in the RAM of the interface circuit board. After the recorded data pattern is completely loaded, it is regenerated at a bit rate controlled by an external clock. The regenerated data pattern now becomes a continuous waveform and is recorded by a Nakamichi M-O disk drive [16].

After the data pattern is recorded, it is read back and sampled by a high speed digitizing scope at 20 MS/s with 16 bits per sample. The sampled waveform data are then transferred back to the computer where we can analyze the readback signal and characterize the ISI. In addition to the 20 MS/s sampling rate, all the experiments were performed at the write power of 5.0 mW, read power of 1.8 mW, constant linear velocity of 4.0 m/s, and diffraction limit (spot size) of 996 nm ($\approx$ 1.0 μm).

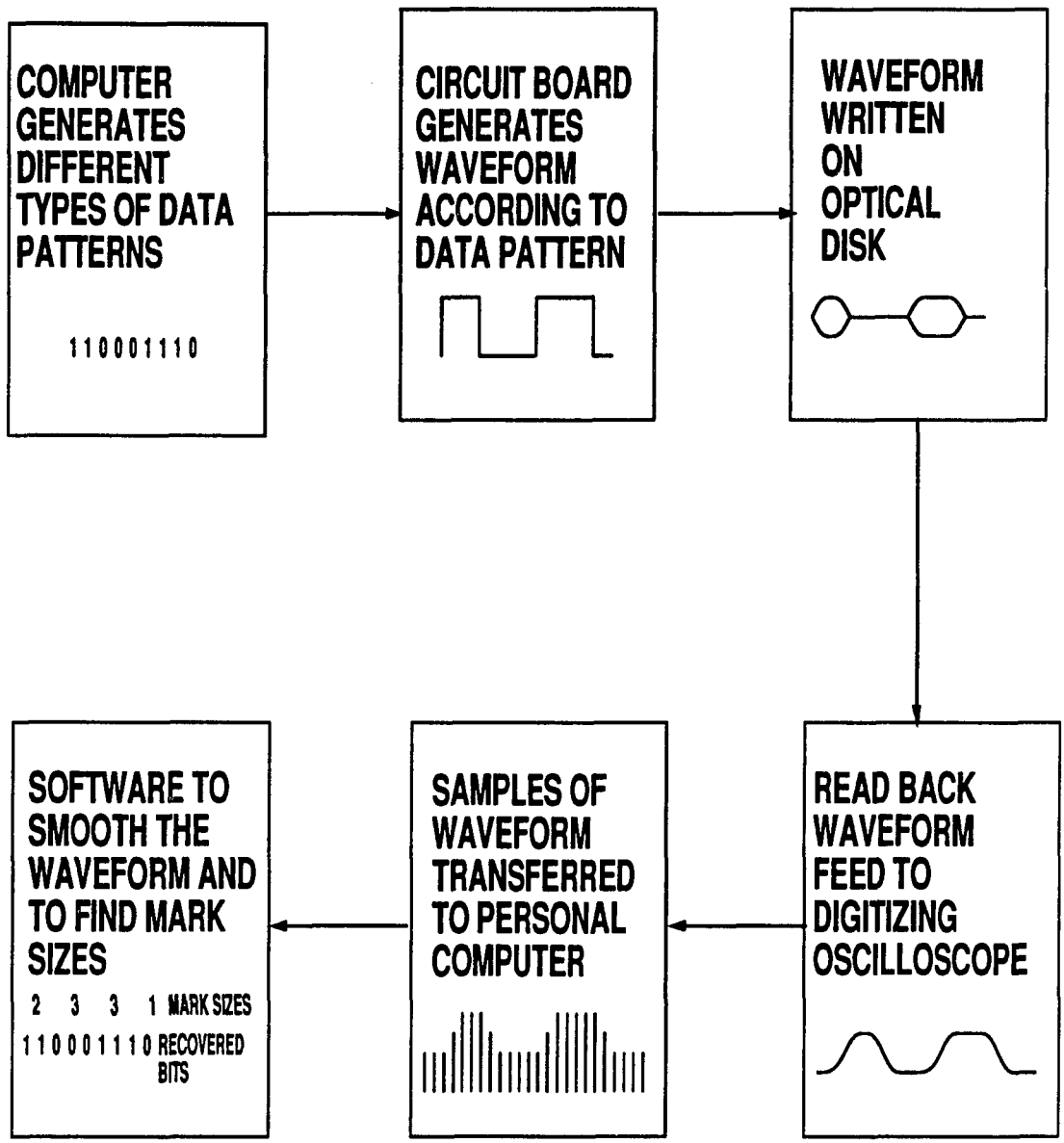

Figure 3.1: ISI Characterization Setup.

3.2 Data Patterns Recorded in the Experiments

To characterize ISI, we need to obtain ISI of a given mark as a function of the widths of itself and neighboring marks. Since there can be a large number of combinations of different mark sizes, we assume ISI of a given mark is a function of only the mark sizes of itself and its two closest neighboring marks. In other words, we neglect the ISI due to farther away neighboring marks. From the experimental results discussed in the next section, we found this is a reasonable assumption. In the following, we will describe various data patterns recorded for ISI characterization.

3.2.1 High Mark ISI Characterization

The first type of ISI is a high mark (laser is turned on) surrounded by two low marks. Fig. 3.2 illustrates a high mark of 1 μm in the middle surrounded by two low marks of 3 μm and 4 μm respectively. Similarly Fig. 3.3 shows the raw waveform for the case when the middle mark is high mark of 1μm and the two adjacent marks are low marks of sizes 1μm each. In the experiments, nT and mT of the two neighboring marks vary from T to $6T$.

3.2.2 Low Mark ISI Characterization

The second type of ISI is a low mark (laser is turned off) surrounded by two high marks. Fig. 3.4 illustrates a low mark of 1 μm in the middle surrounded by two high marks of 2 μm and 4 μm respectively. In the experiments, nT and mT of the two neighboring marks vary from T to $6T$.

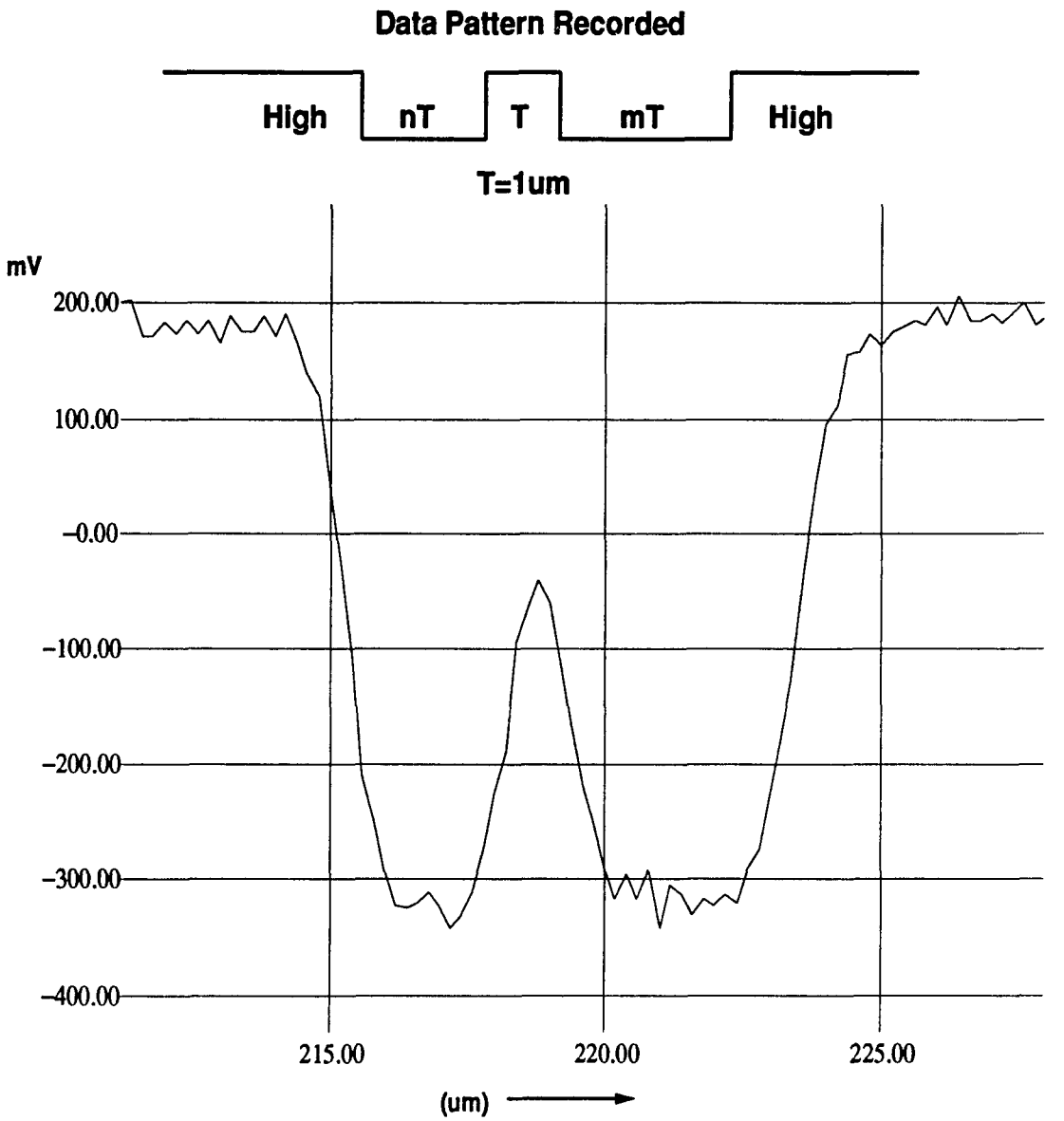

Figure 3.2: Read Back Raw Waveform for n=3 and m=4.

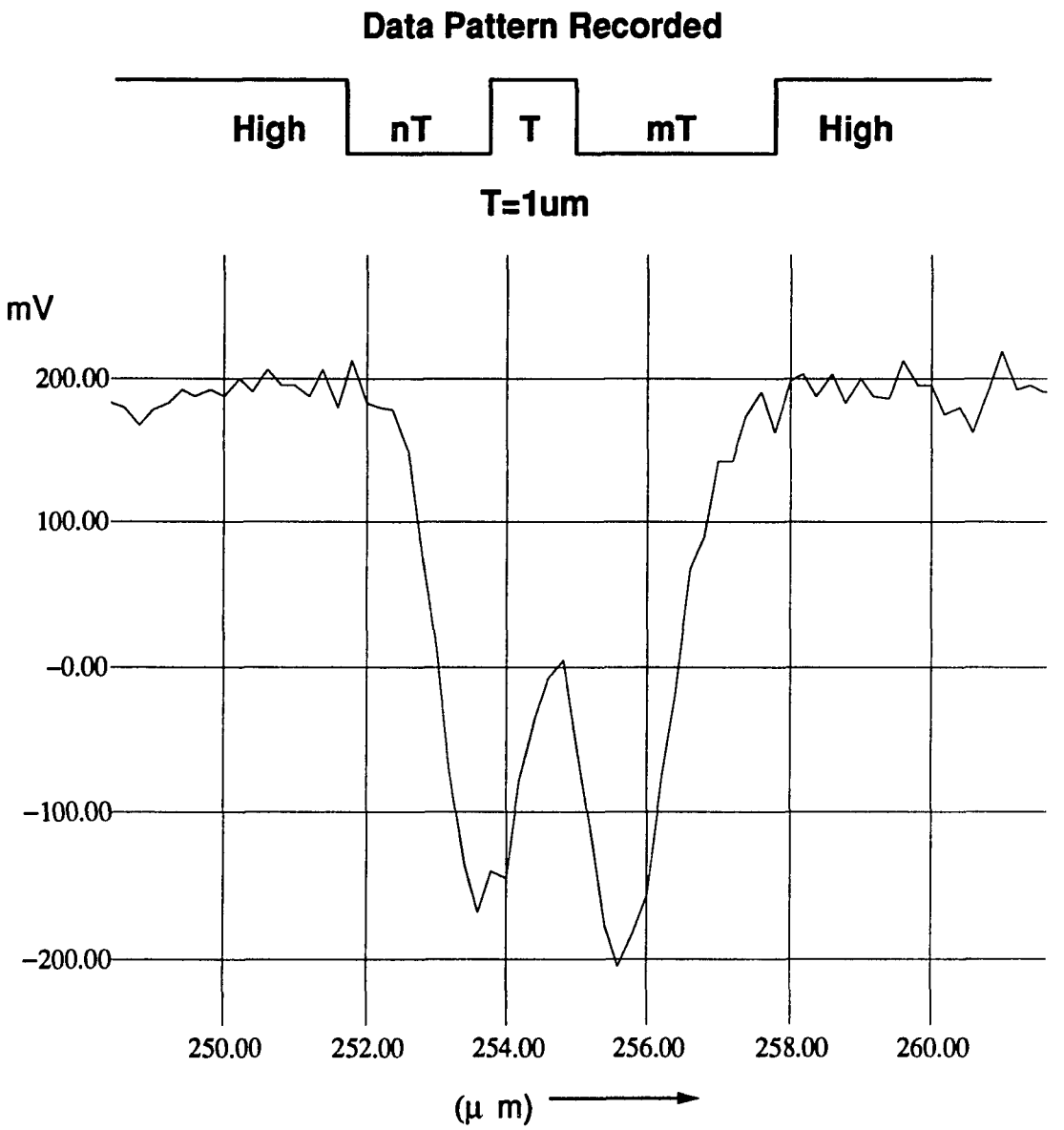

Figure 3.3: Read Back Raw Waveform for n=1 and m=1.

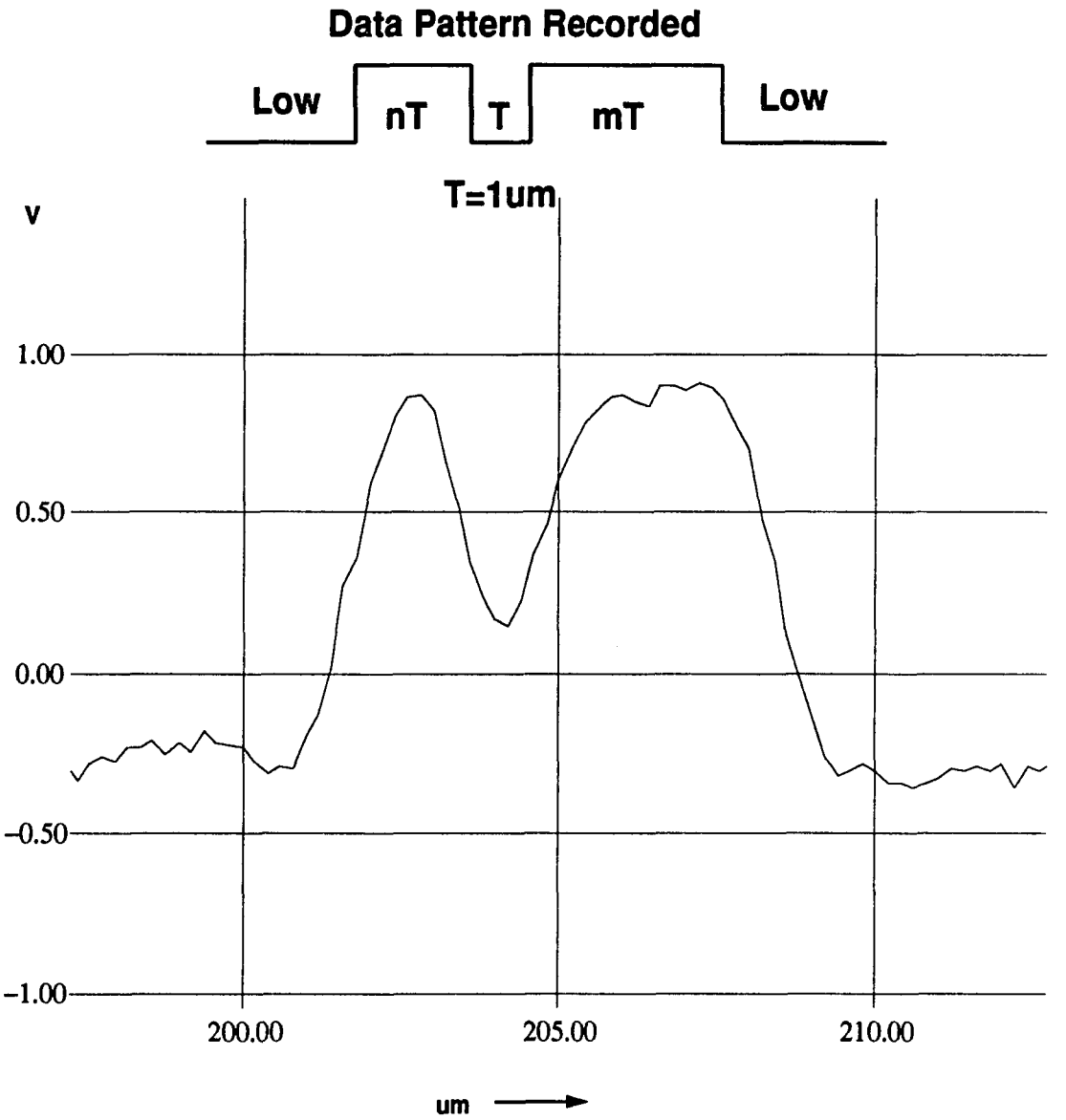

Figure 3.4: Read Back Raw Waveform for n=2 and m=4.

3.2.3 ISI of Isolated Marks

When n and m of the two neighboring marks described above become very large (i.e. , $n, m \rightarrow \infty$), the middle mark becomes an isolated mark. To understand this limiting case, we also recorded isolated marks of various sizes. Fig. 3.5 illustrates the isolated high mark of width 3μm and Fig. 3.6 illustrates the isolated low mark of width 1μm.

3.2.4 Pseudo Random Sequence

A pseudo random sequence is also recorded for SNR computation. The sequence has a period of 31 data bits which generates a random pattern of low and high marks. This pseudo random waveform is to simulate low and high marks as encountered in practical data storage system.

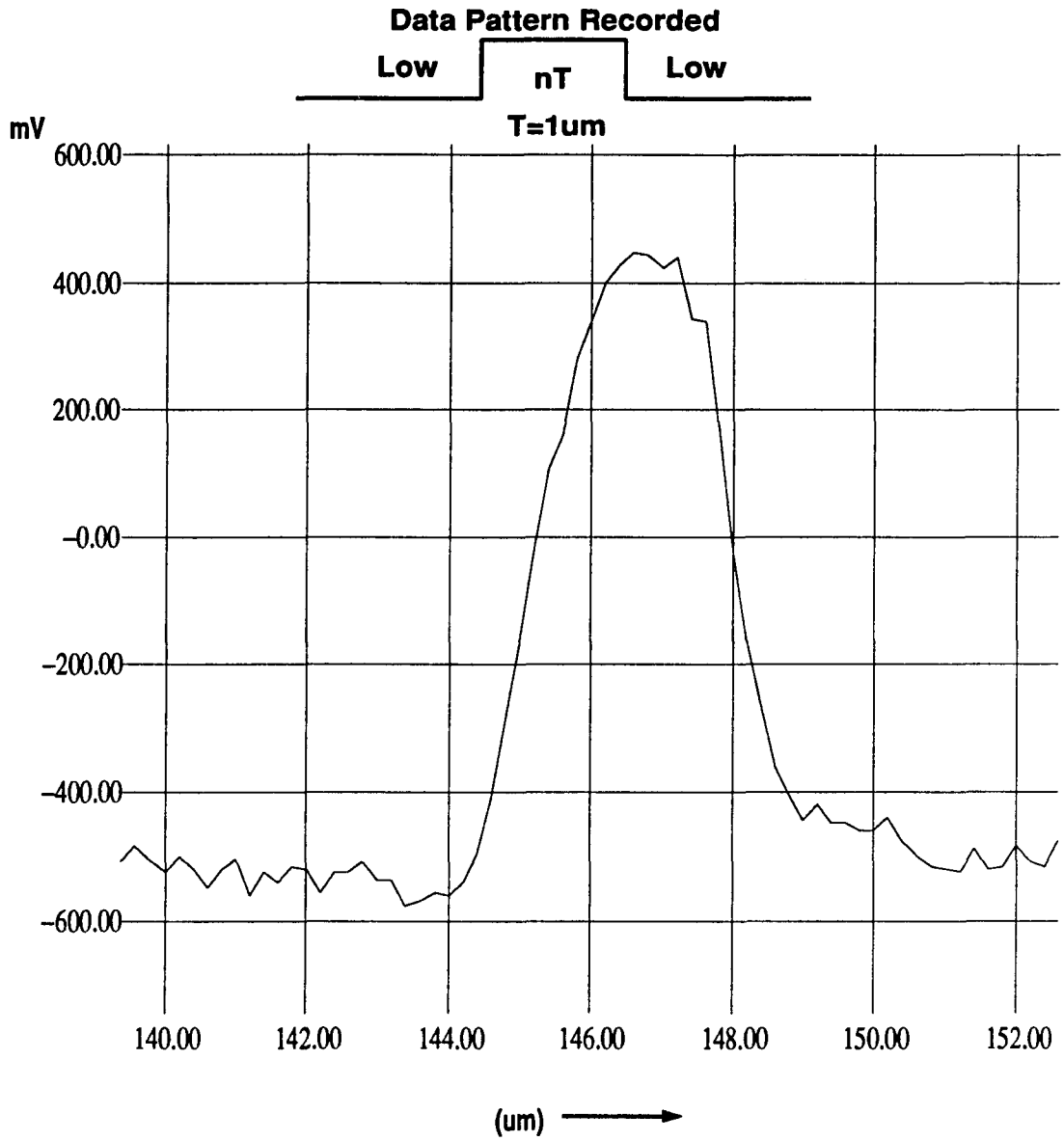

Figure 3.5: Read Back Raw Waveform for n=3.

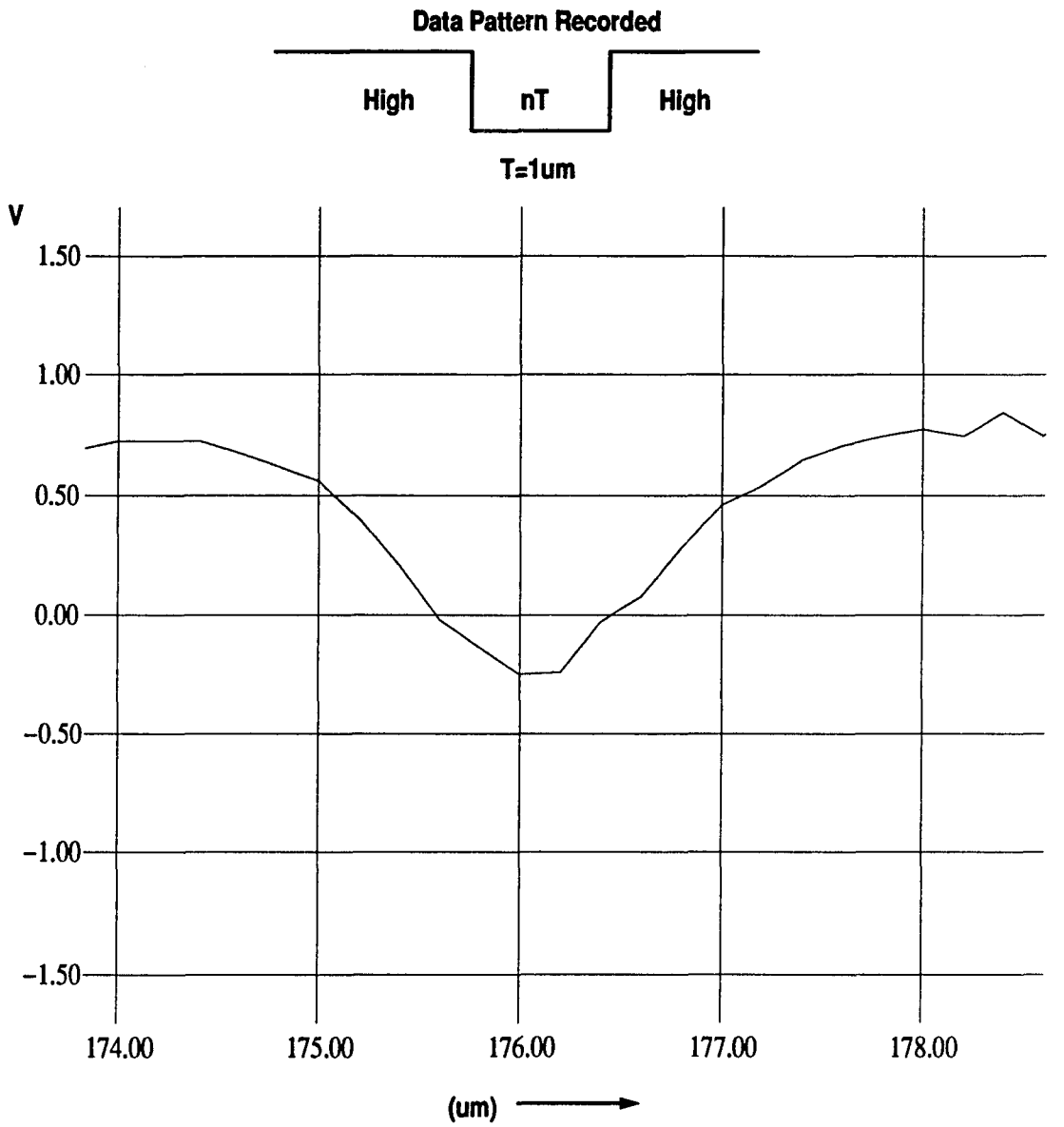

Figure 3.6: Read Back Raw Waveform for n=1.

CHAPTER 4

Data Analysis and ISI Characterization

Once a recorded data pattern is read back and sampled, the first step in data analysis is to compute the width of each individual mark. Since the sampled waveform for each data pattern consists of not only ISI but also random noise, we need to take average of the repetitive data patterns to suppress the noise. In this chapter, we will explain these steps and quantify the ISI with an empirical interpolation function.

4.1 Mark Size Detection

After the read back signal is sampled, mark sizes are detected with the help of a computer program, which computes each mark size by detecting its two boundaries. The basic idea used in the program for boundary detection is to take first and second derivatives of the readback signal. As illustrated in Fig. 4.1, peaks of the first derivative and zero-crossings of the second derivatives correspond to the mark boundaries. By matching the peaks and zero-crossings, we can easily find the mark boundaries and consequently the mark widths. Since the readback signal is discrete after sampling, we will explain below how to regenerate a smooth curve for the readback signal and to find the first and second derivatives.

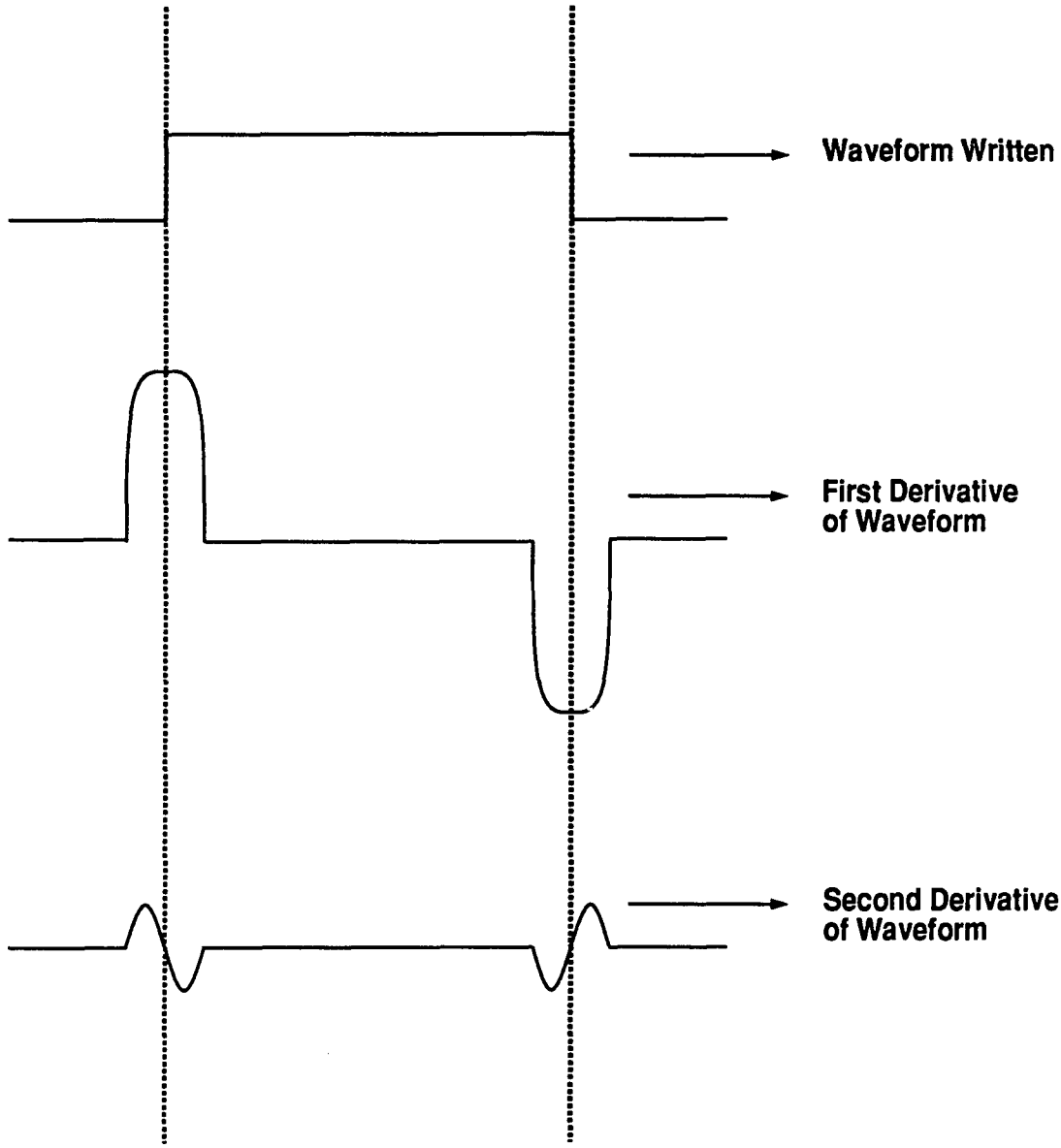

Figure 4.1: Mark Size Detection Method.

First, let y_i be the amplitude of the i^{th} data point of the original waveform, and let x_i be the time point corresponding to the data point y_i. For computational convenience, x_i is actually set to zero so we do not have to know the *absolute position* of the sample data. The basic idea of curve smoothing or curve fitting is to find the coefficients a_2, a_1, and a_0 for a given point x_i such that

$$\hat{y}_{i+k} = a_2 x_{i+k}^2 + a_1 x_{i+k} + a_0 \tag{4.1}$$

$$= \sum_{j=0}^{2} a_j x_{i+k}^j. \tag{4.2}$$

is as close to y_{i+k} as possible for $k = 0, \pm 1, \ldots \pm 5$. More quantitatively, the coefficients a_j's are determined for each data point by minimizing the square sum:

$$\sum_{k=-5}^{5} (y_{i+k} - \hat{y}_{i+k})^2.$$

Detailed derivation of this minimum mean square interpolation is given in Appendix A.

Once we obtain the coefficients a_j's for each data point y_i, we can find its first and second derivatives to detect the mark boundaries. From Eq. (4.1), we have

$$\dot{y}_i = 2a_2 x_i + a_1 \tag{4.3}$$

and

$$\ddot{y}_i = 2a_2 \tag{4.4}$$

where $\dot{y}_i$ is the value of the first derivative corresponding to x_i, and $\ddot{y}_i$ is the value of second derivative corresponding to x_i. Figs. 4.2, 4.3, 4.4, 4.5 and 4.6 show the smoothed waveform, and the first and second derivatives of Figs. 3.2, 3.4, 3.5 and 3.6, respectively.

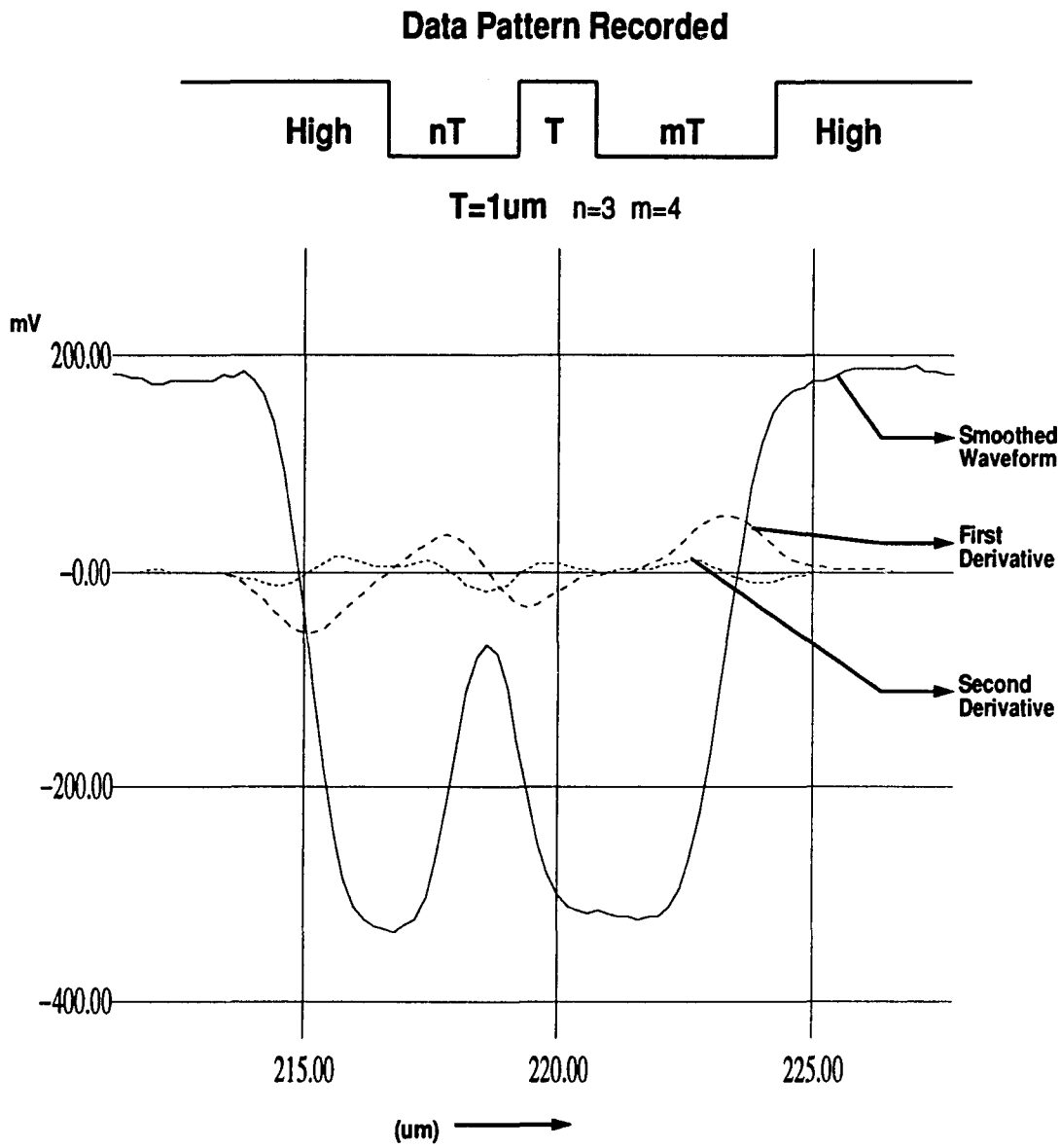

Figure 4.2: Smoothed Waveform, First and Second Derivatives of Fig. 3.2.

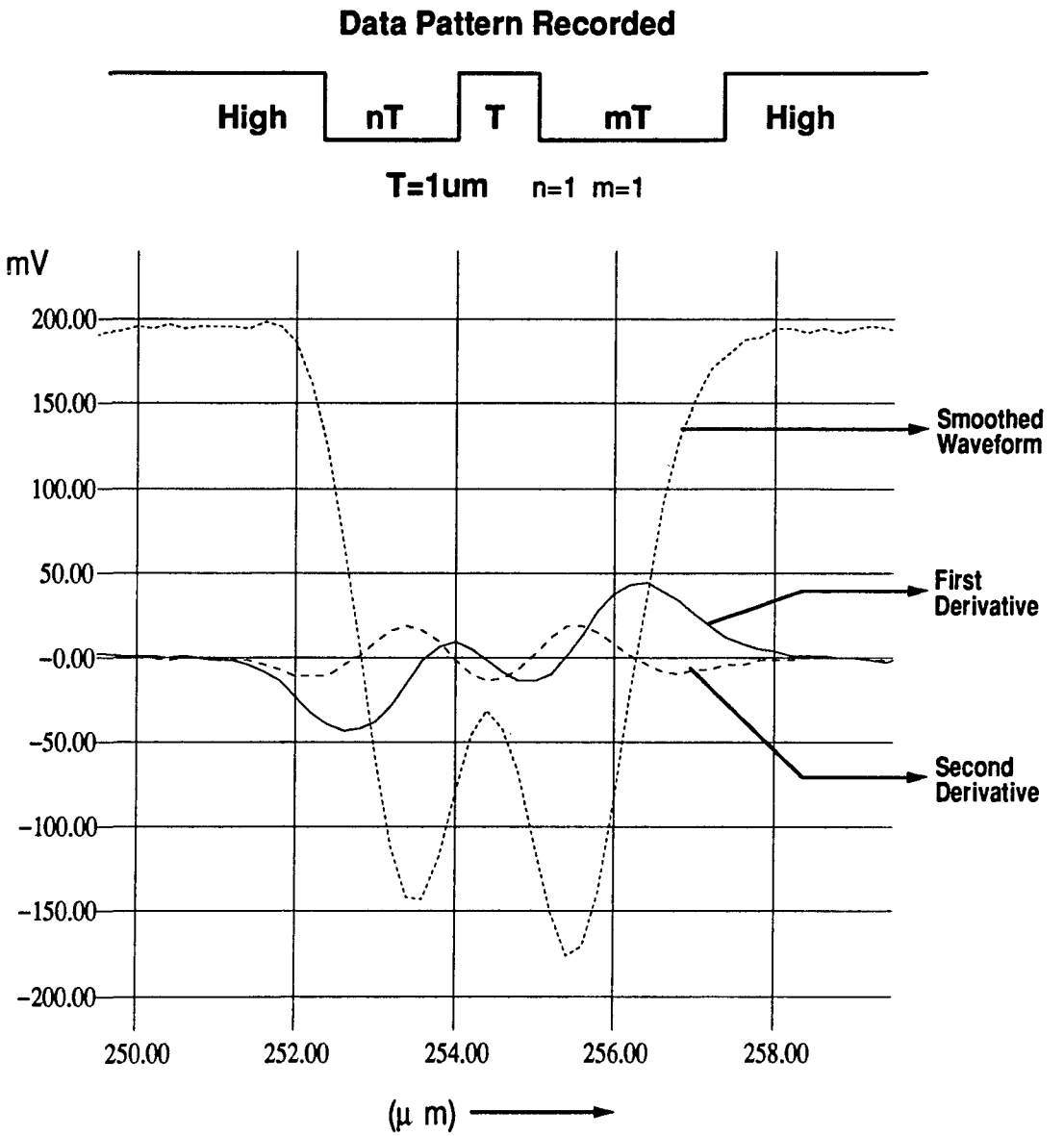

Figure 4.3: Smoothed Waveform, First and Second Derivatives of Fig. 3.3.

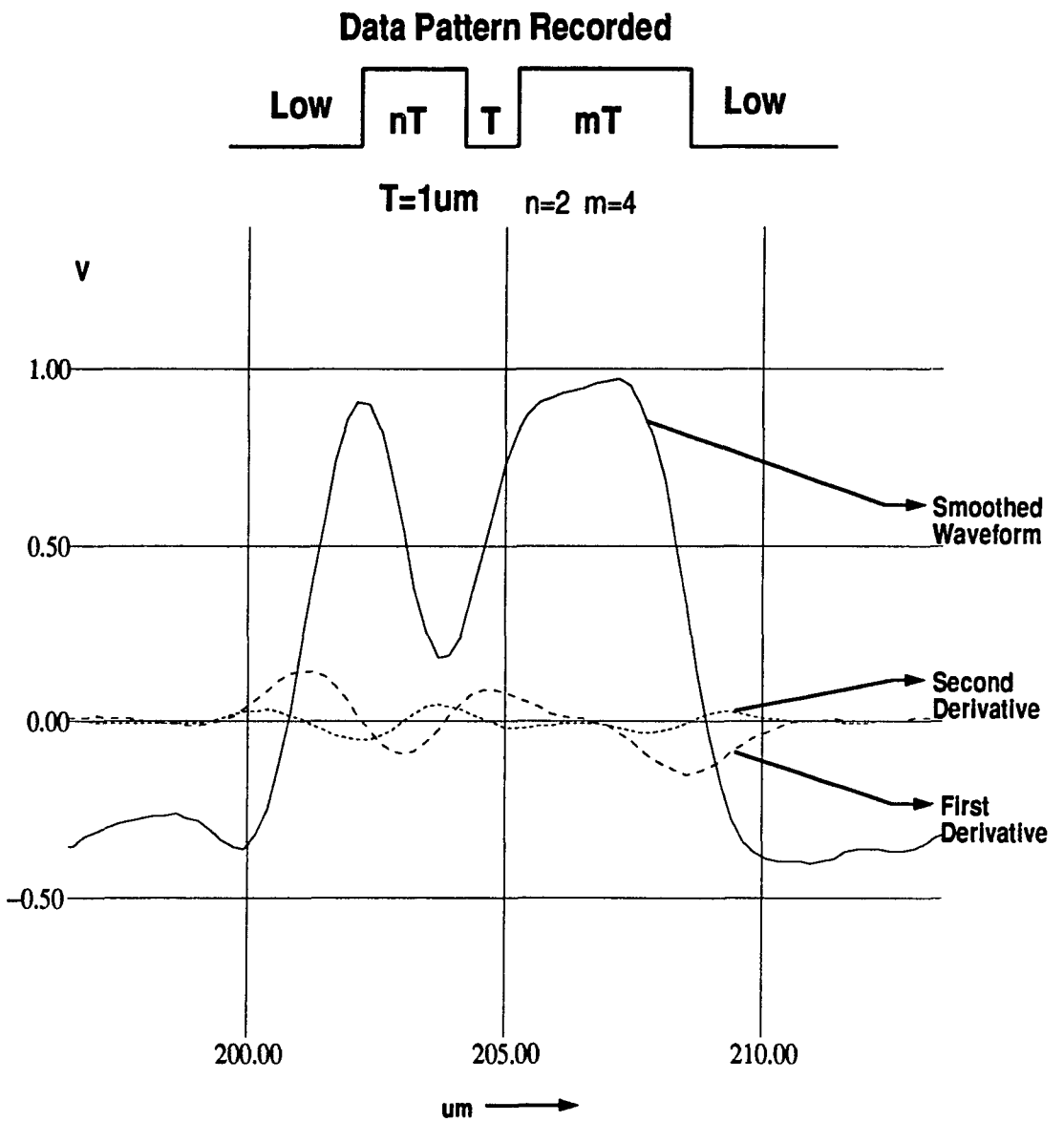

Figure 4.4: Smoothed Waveform, First and Second Derivatives of Fig. 3.4.

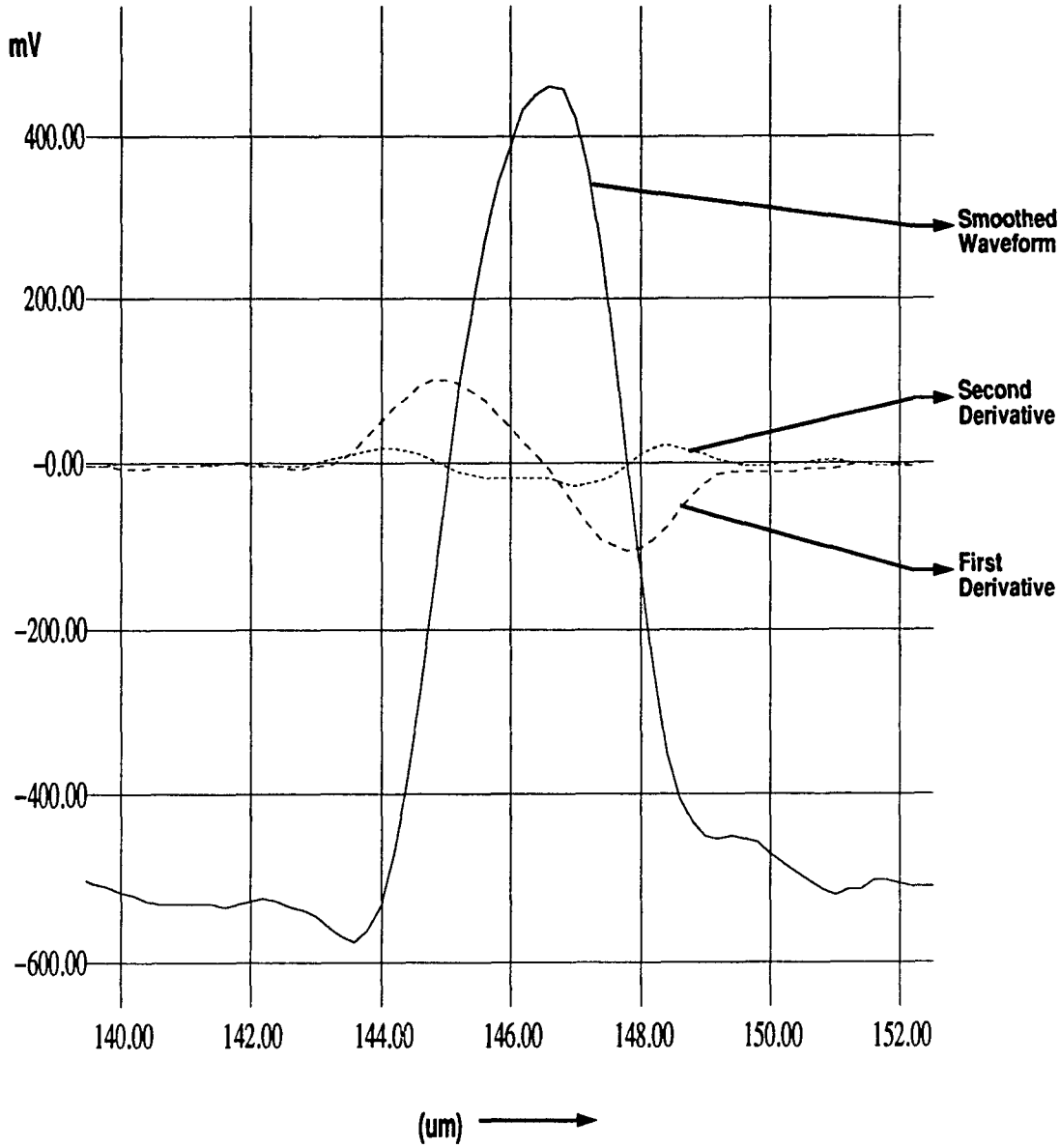

Figure 4.5: Smoothed Waveform, First and Second Derivatives of Fig. 3.5.

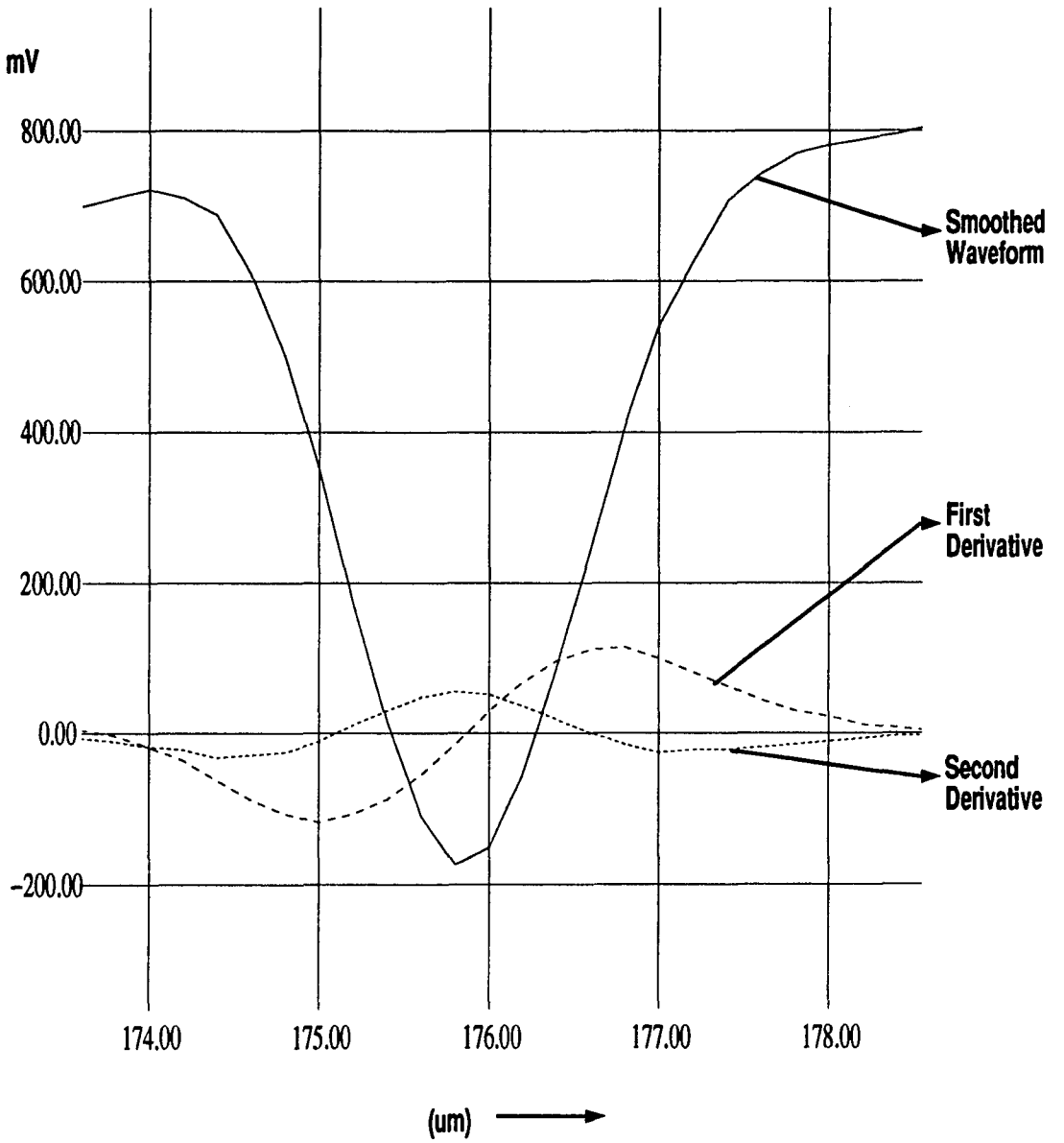

Figure 4.6: Smoothed Waveform, First and Second Derivatives of Fig. 3.6.

Once we compute each mark width, we compute a large number of mark widths of the same pattern and take the average to suppress random noise. The ISI will be simply the deviation of the averaged mark width from its original recorded width. Results of these computations are summarized in the next section.

4.2 ISI Characterization

From the computed mark widths of different patterns, we can characterize the ISI for the given M-O system. Since ISI is a function of the mark polarization and also a function of the widths of the center mark and its two neighboring marks, we consider four cases as summarized below.

4.2.1 ISI Characteristics for High Center Marks

Fig. 4.7 shows the first type of ISI characteristics where the center mark is a high mark. Each ISI curve shown in the figure is a function of the width of the right neighboring mark, at a fixed width of the left neighboring mark. The width of the center mark is fixed at 1 μm. From the results we can see that the ISI behavior is highly non-linear. When the adjacent marks are greater than 2 μm, the ISI approaches a constant value.

4.2.2 ISI Characteristics for Low Center Marks

Fig. 4.8 shows the second type of ISI characteristics where the center mark is a low mark. The ISI curves are plotted very similar to that in the first case. We can see that the nature of ISI behavior for this case is very similar to that of the previous case.

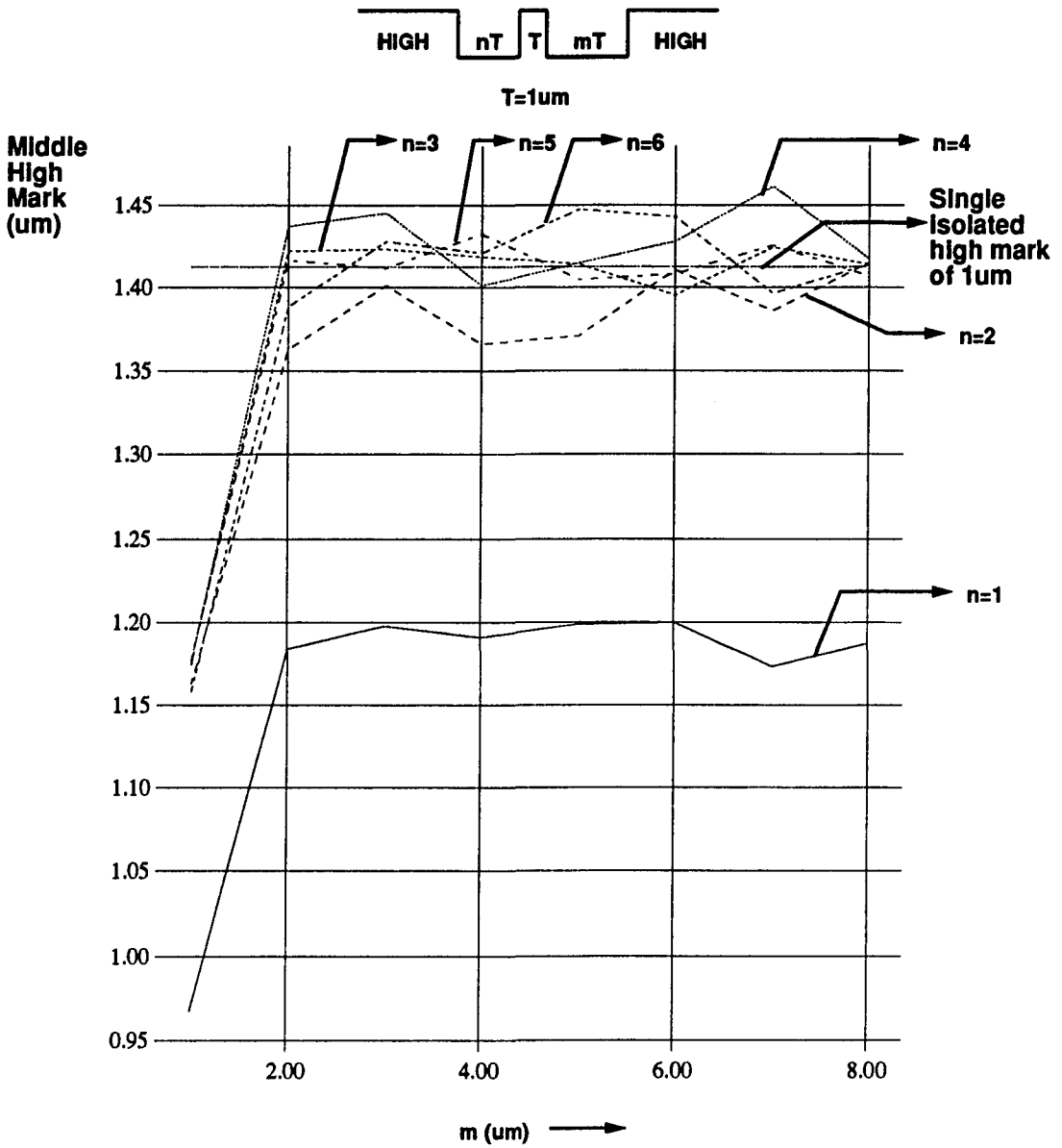

Figure 4.7: ISI Characteristics for High Center Marks.

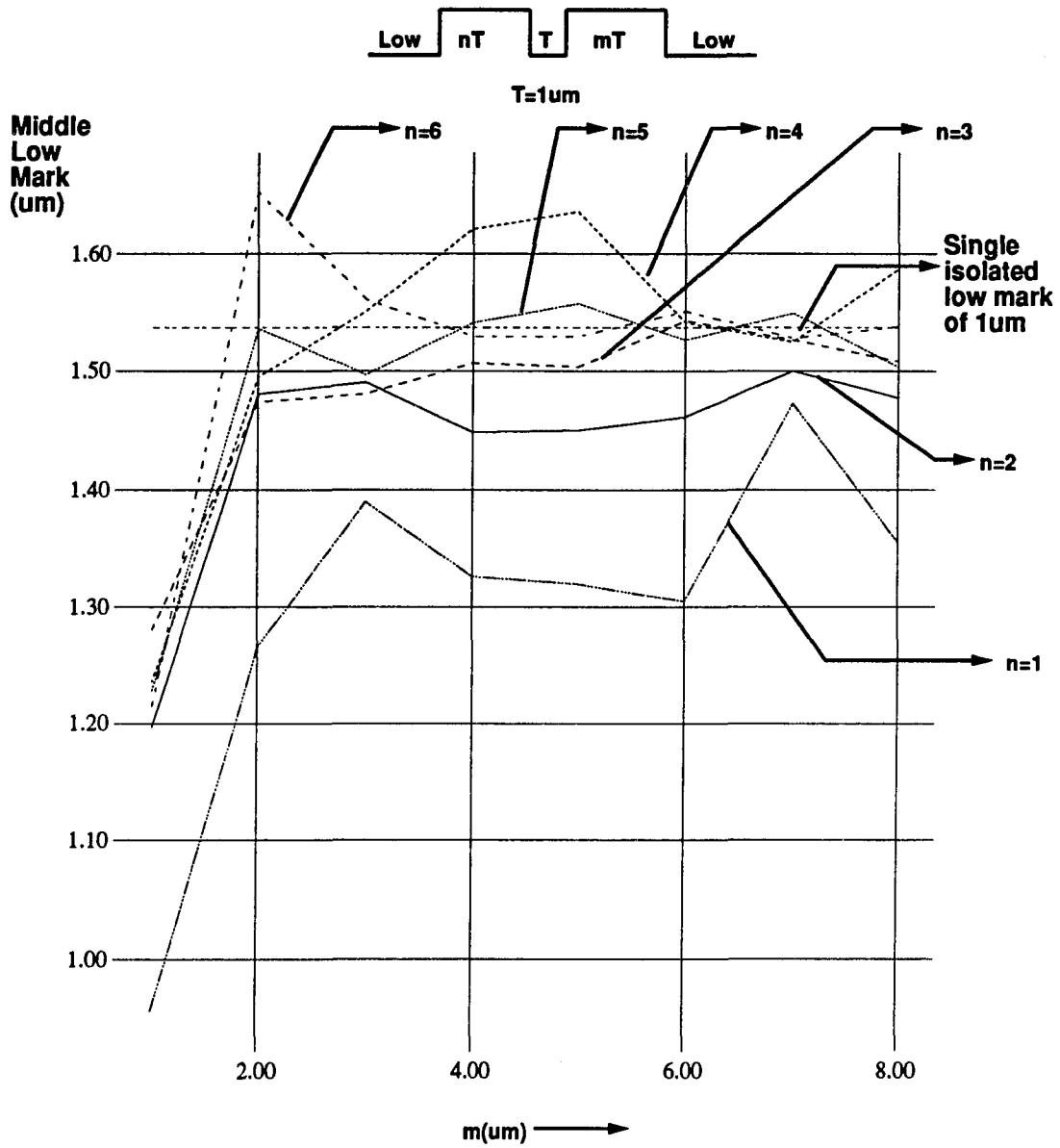

Figure 4.8: ISI Characteristics for Low Center Marks.

4.2.3 ISI Characteristics for Isolated High Center Marks

In the first two types of the ISI characteristics summarized, the center mark is fixed at 1 μm. In this third case, the width of the center mark is a variable with large neighboring marks. Therefore, the center mark is essentially an isolated mark. Fig. 4.9 illustrates the difference between a recovered isolated high mark and recorded mark as a function of width of the recorded high mark. From the figure, we see that ISI is positive for marks less than 1.5 μm and negative for marks greater than 1.5μm. ISI approaches zero as the mark size increases.

4.2.4 ISI Characteristics for Isolated Low Center Marks

This case is similar to the third case except that the center mark is now a low mark. Fig. 4.10 illustrates the difference between a recovered isolated low mark and recorded mark as a function of width of the recorded low mark. From the figure, we see that the ISI value is always positive and approaches zero as the mark size increases.

4.3 Interpolation of ISI Characteristics

To perform simple ISI equalization in the read process, instead of using an ISI table, we may simply use an empirical function that gives an estimated amount of ISI from the detected widths of the center mark and its two neighbors.

By observing the ISI characteristics shown in Figs. 4.7 and 4.8, a simple empirical function is proposed to be of the following form:

$$W(n_l, n_m, n_r) = I(n_m)\left\{\frac{2}{\pi}\arctan([\frac{n_l}{k_1}]^{\alpha})\right\}\left\{\frac{2}{\pi}\arctan([\frac{n_r}{k_1}]^{\alpha})\right\} \tag{4.5}$$

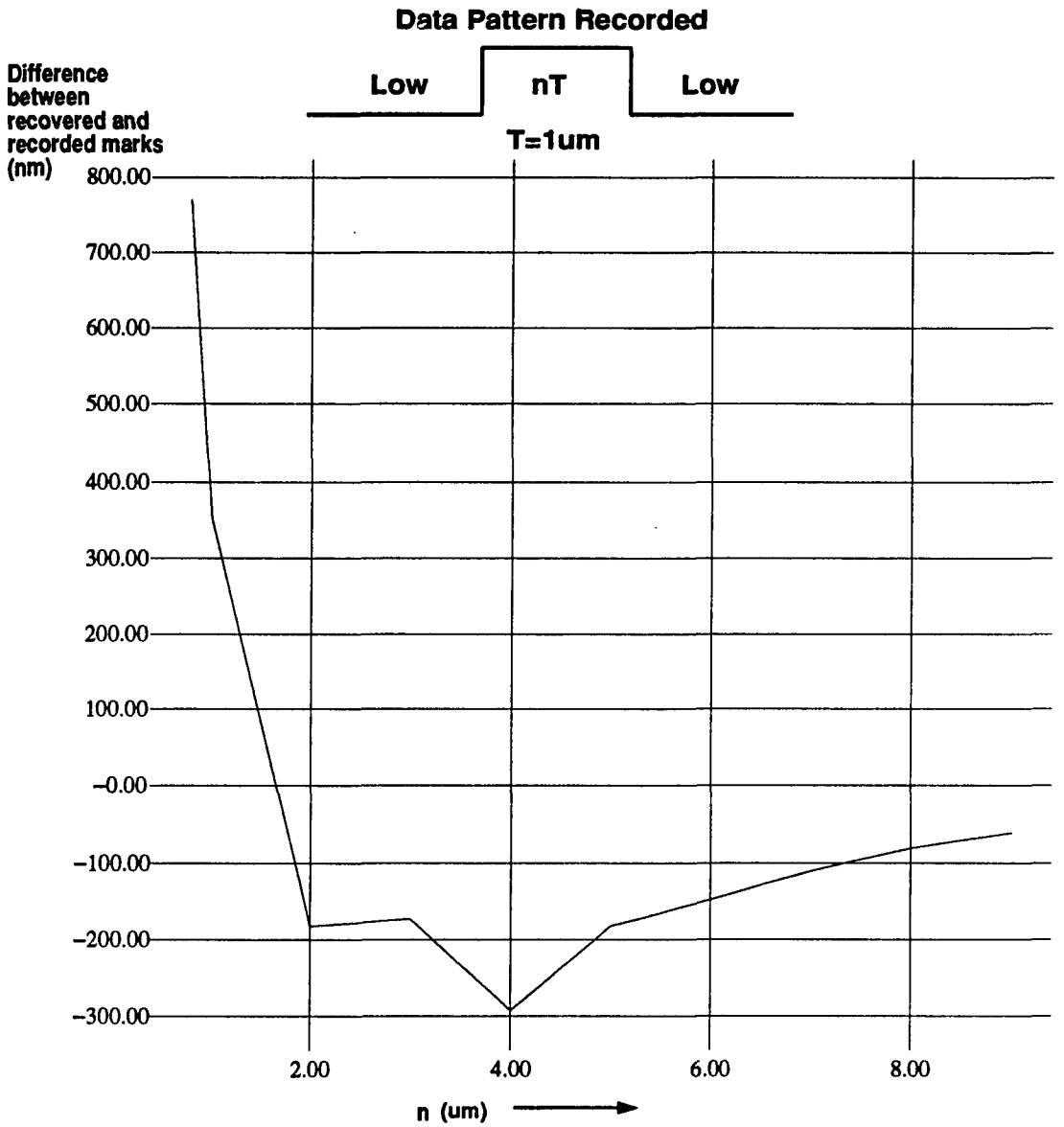

Figure 4.9: ISI Characteristics for Isolated High Center Marks.

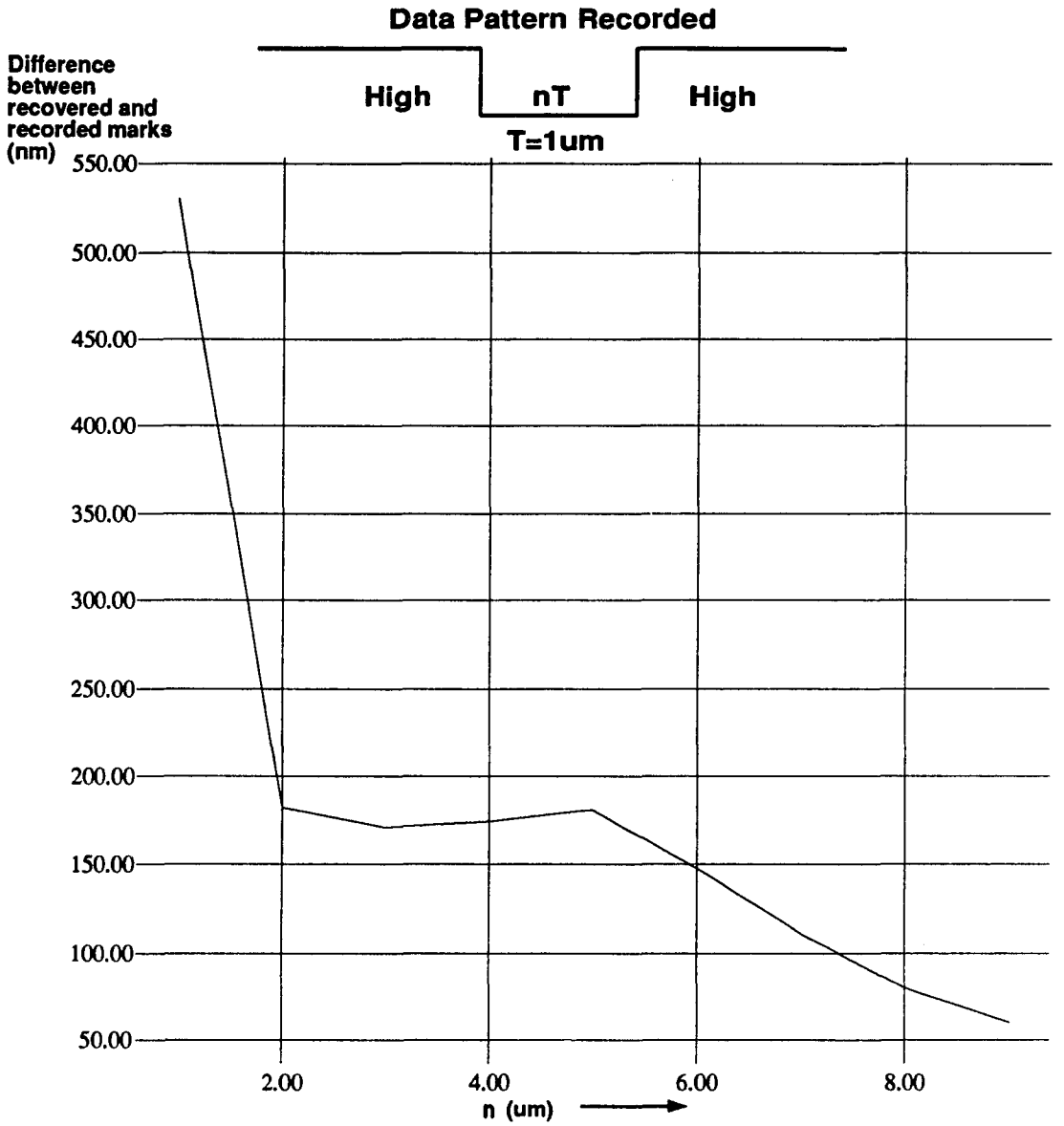

Figure 4.10: ISI Characteristics for Isolated Low Center Marks.

where n_l is the recorded mark width on left side, n_m is the recorded mark width in the middle, n_r is the recorded mark width on the right side, $I(n_m)$ is the width of the isolated mark n_m, and $W(n_l, n_m, n_r)$ is the actual mark width of the center mark. k_1 and α are constants. Therefore, the amount of ISI is determined as

$$ISI(n_l, n_m, n_r) = n_m - W(n_l, n_m, n_r). \tag{4.6}$$

From this empirical function, we can see that when both n_r and n_m are large, the actual mark widths approach the isolated mark width $I(n_m)$. Also, at fixed n_r and n_m, the $W(n_l)$ is an arctan function, which is what we see from the experimental results. In Figs. 4.11 and 4.12, we superimpose the empirical curves on the actual curves according to Eq. (4.5).

The constants k_1 and α are determined as follows:

First we normalize the actual mark widths $W(n_l, n_m, n_r)$ by dividing them by the width of the isolated mark $I(n_m)$.

We then set particularly two values:

$$\frac{2}{\pi}\arctan([\frac{2.0}{k_1}]^{\alpha}) = \frac{W(n>1, n_m, n_r=2)}{I(n_m)} \tag{4.7}$$

$$\frac{2}{\pi}\arctan([\frac{1.0}{k_1}]^{\alpha}) = \frac{W(n=1, n_m, n_r>>2)}{I(n_m)}. \tag{4.8}$$

From Eqs. 4.7 and 4.8 we solve for k_1 and α whose expressions are given below.

Defining two new parameters a and b as

$a = W(n>1, n_m, n_r=2)/I(n_m)$ and

$b = W(n=1, n_m, n_r>>2)/I(n_m)$,

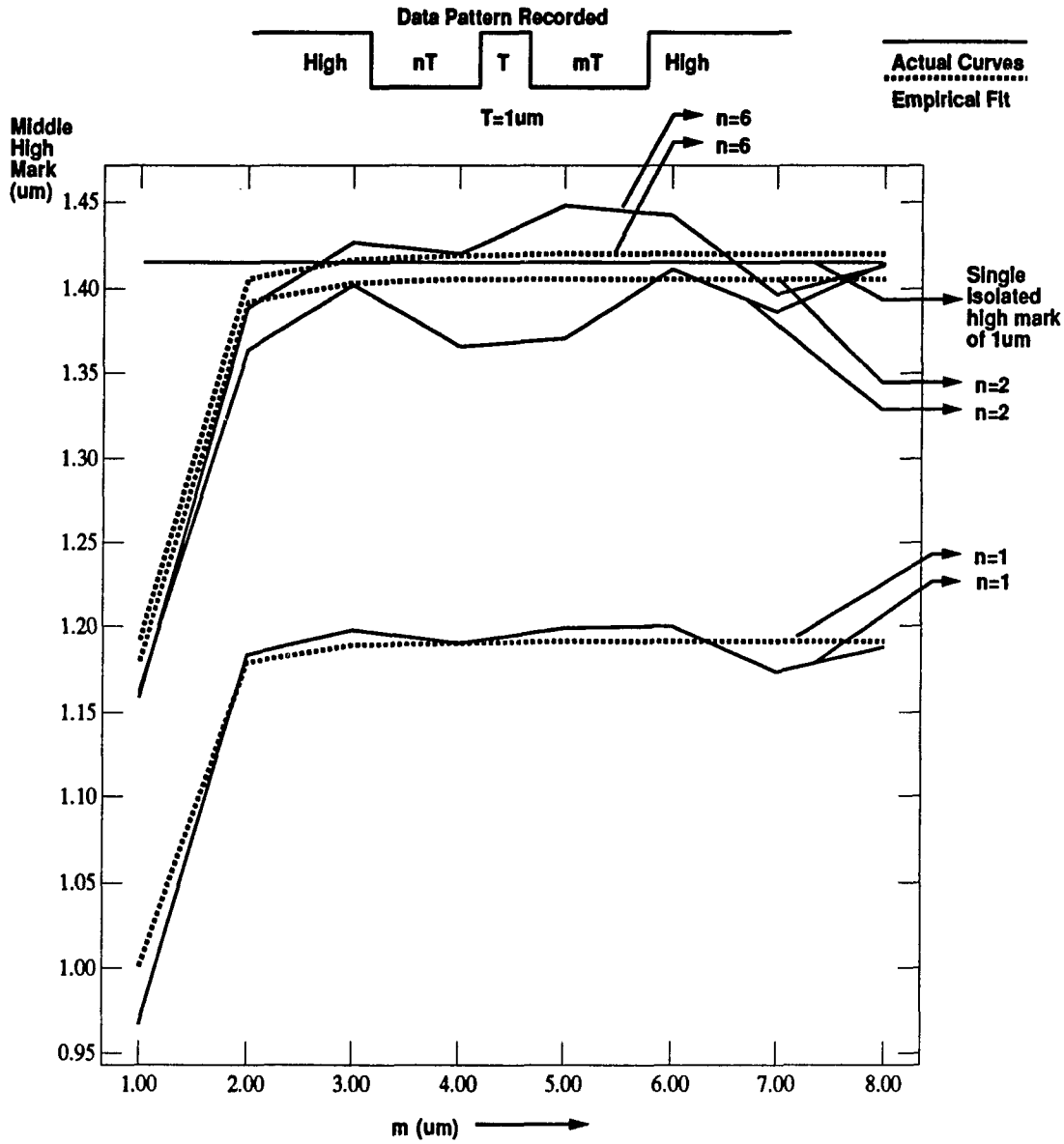

Figure 4.11: Superimposition of Actual and Empirical Curves of ISI for High Marks.

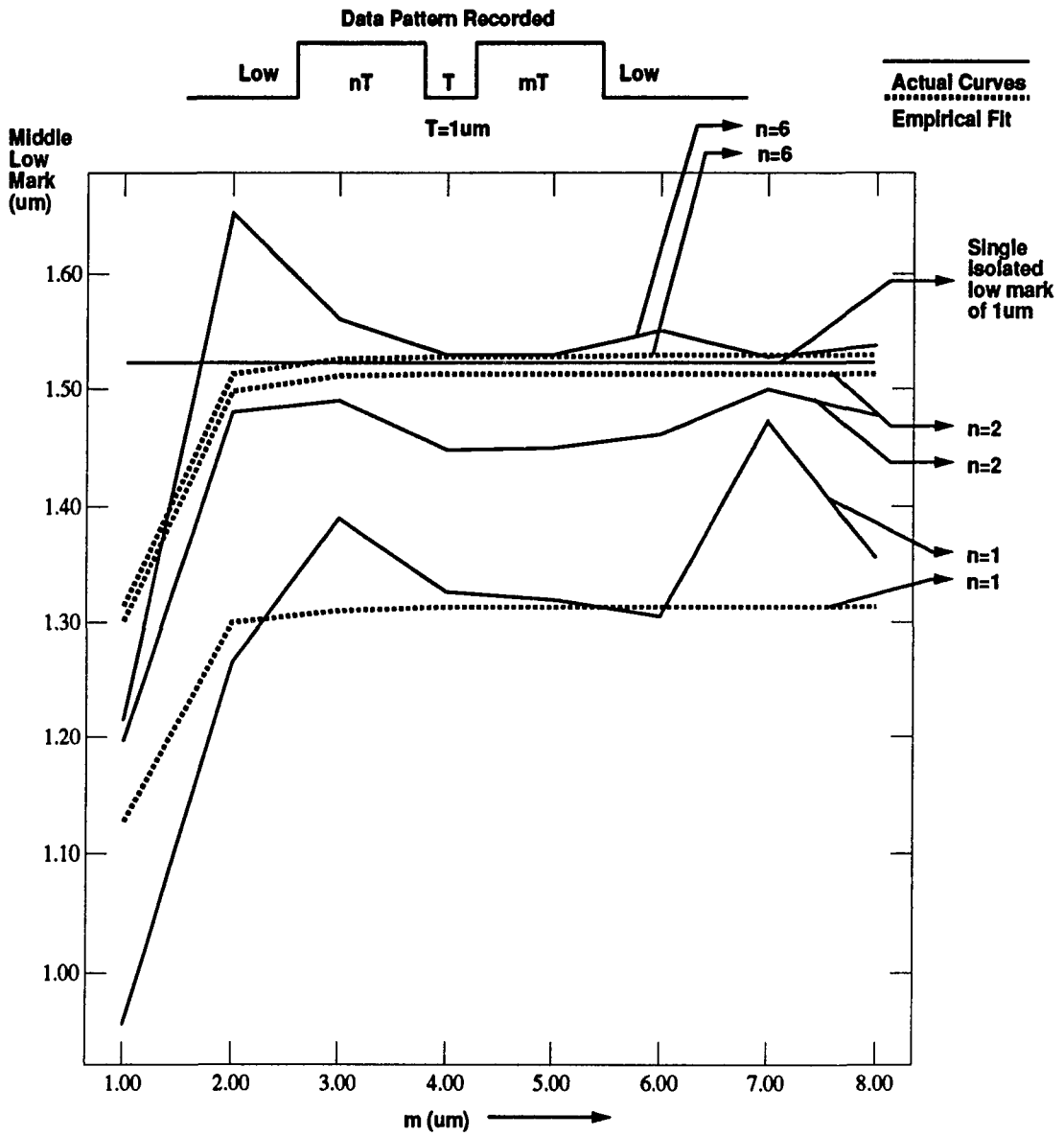

Figure 4.12: Superimposition of Actual and Empirical Curves of ISI for Low Marks.

the equations for α and k_1 become

$$\alpha = \log(\frac{\tan(a\frac{\pi}{2})}{\tan(b\frac{\pi}{2})})/\log(2.0) \tag{4.9}$$

and

$$k_1 = 1.0/\{\tan(b\frac{\pi}{2})\}^{\frac{1}{\alpha}}. \tag{4.10}$$

In Fig. 4.11, $\alpha = 3.039685$ and $k_1 = 0.640727$ μm, and in Fig. 4.12, $\alpha = 2.801347$ and $k_1 = 0.581585$ μm.

CHAPTER 5

SNR Computation With and Without Equalization

Once we know the ISI characteristics, we can use equalization to see how much SNR can be improved. To compute SNR, a pseudo random sequence of length 31 data bits is used as the testing data pattern. In the following, we explain the SNR computation process and plot SNR as a function of the minimum mark size of the given data pattern. As explained in the experimental setup, we can use different clock rates to record the same random pattern with different minimum mark sizes.

Fig. 5.1 shows the pseudorandom sequence recorded and the corresponding readback smoothed waveform when the minimum mark size is of 1μm. Fig. 5.2 shows the first and second derivatives of the pseudorandom sequence of Fig. 5.1

The computation of SNR can be understood as follows:

Let W_1, W_2, W_3, $\cdots$, W_N be the mark widths recorded on optical disk.

Let $\hat{W}_1$, $\hat{W}_2$, $\hat{W}_3$, $\cdots$, $\hat{W}_N$ be the marks recovered from the readback signal.

Let d_1, d_2, d_3, $\cdots$, d_N be the difference between W_i and $\hat{W}_i$. Then we have

$$d_i = W_i - \hat{W}_i; \qquad i = 1, 2, \cdots N. \tag{5.1}$$

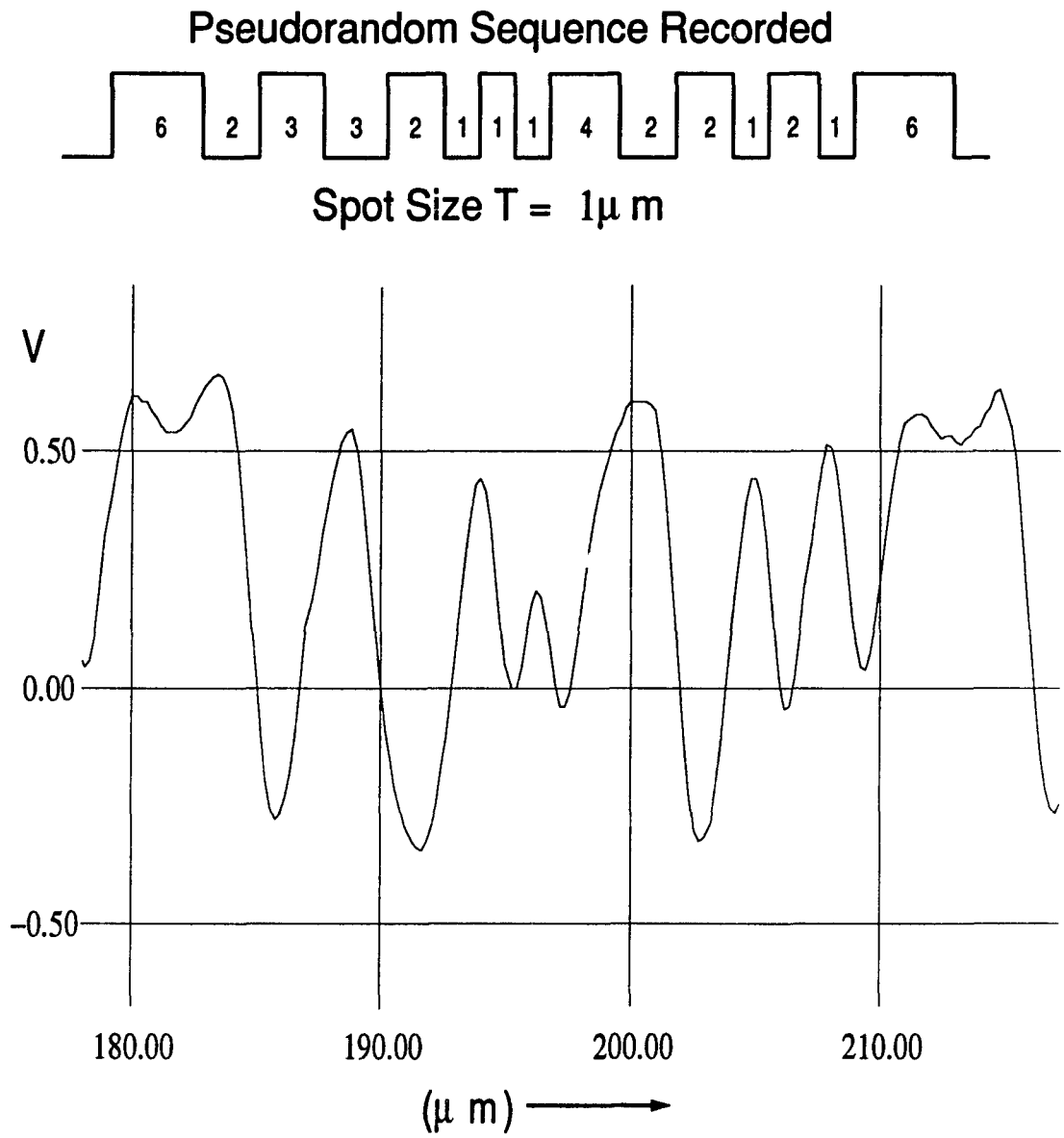

Figure 5.1: Smoothed Waveform of Pseudorandom Sequence.

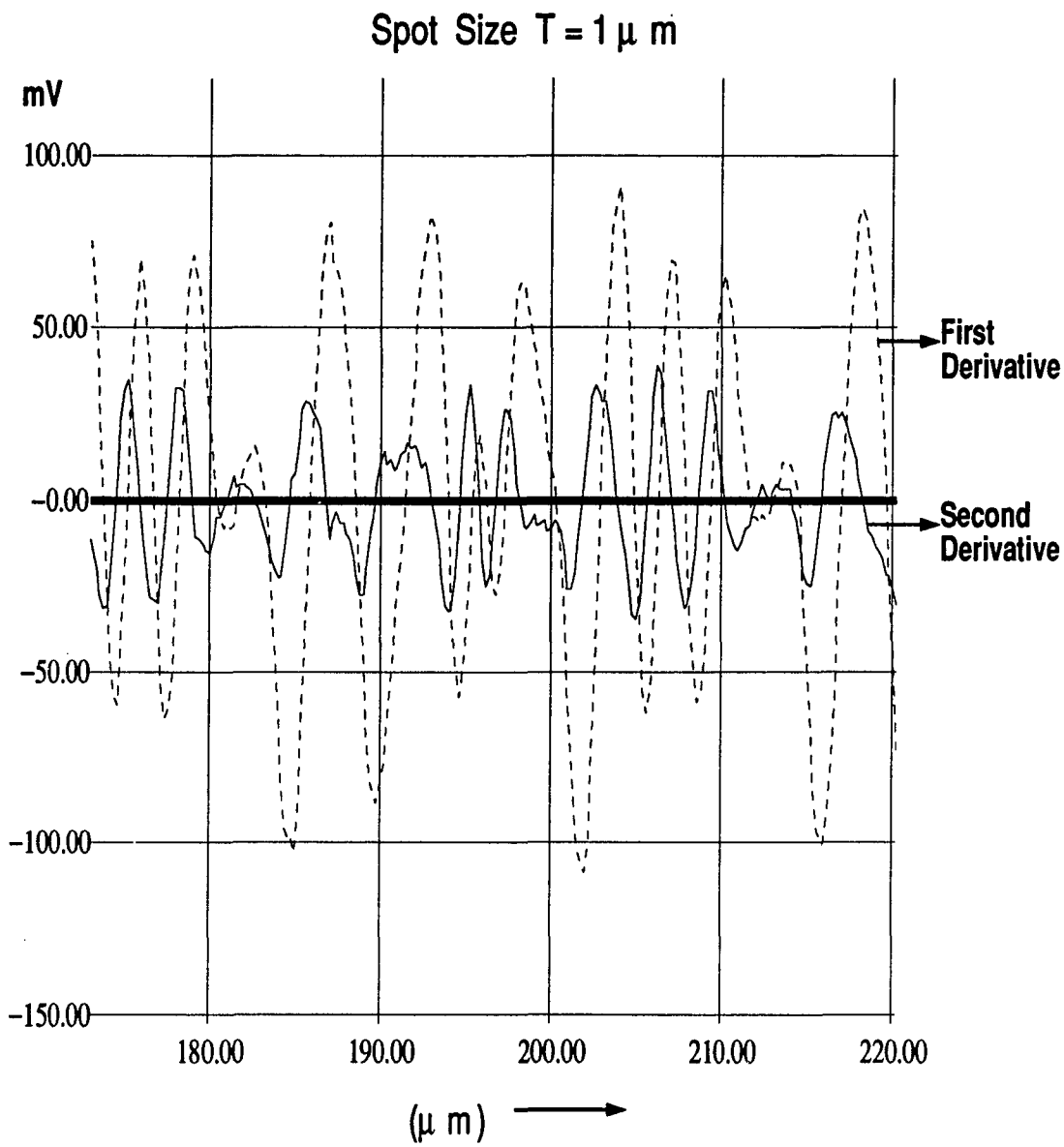

Figure 5.2: First and Second Derivatives of the Pseudorandom Sequence.

The variance is defined as

$$\sigma^2 = \frac{1}{N}\sum_{i=1}^{N} d_i^2. \tag{5.2}$$

Therefore, SNR is

$$SNR = 10\log_{10}(\frac{W_{unit}^2}{\sigma^2}) \tag{5.3}$$

where W_{unit} is the width of the minimum mark size recorded.

From Eqs. (5.1)- -(5.3), various kinds of SNR's can be obtained. Fig. 5.4 gives SNR as a function of the minimum mark width. As shown in the figure, there are four different SNR curves. The high mark SNR curve is obtained by computing the variance using only the high marks. Similarly, the low mark SNR curve considers only the low marks, and the all mark SNR considers all marks. The fourth SNR curve uses the Additive Interleaving Detection (AID) [11], where each "mark width" W_i or $\hat{W}_i$ is the sum of two adjacent marks of opposite polarization. That is, we use

$$\Xi\ W_j = W_j + W_{j+1} \tag{5.4}$$

as the mark size for variance and SNR computations. Fig. 5.3 shows the Additive Interleaving Detection (AID) method.

All the four SNR curves in Fig. 5.4 are obtained without ISI equalization. Fig. 5.5 shows the SNR after equalization. Equalization was performed using the empirical relation developed in Eqs. (4.5) and (4.6).

From Fig. 5.4; we can see that as minimum mark size increases, the SNR increases. The SNR using AID method was considerably better than those without using equalization

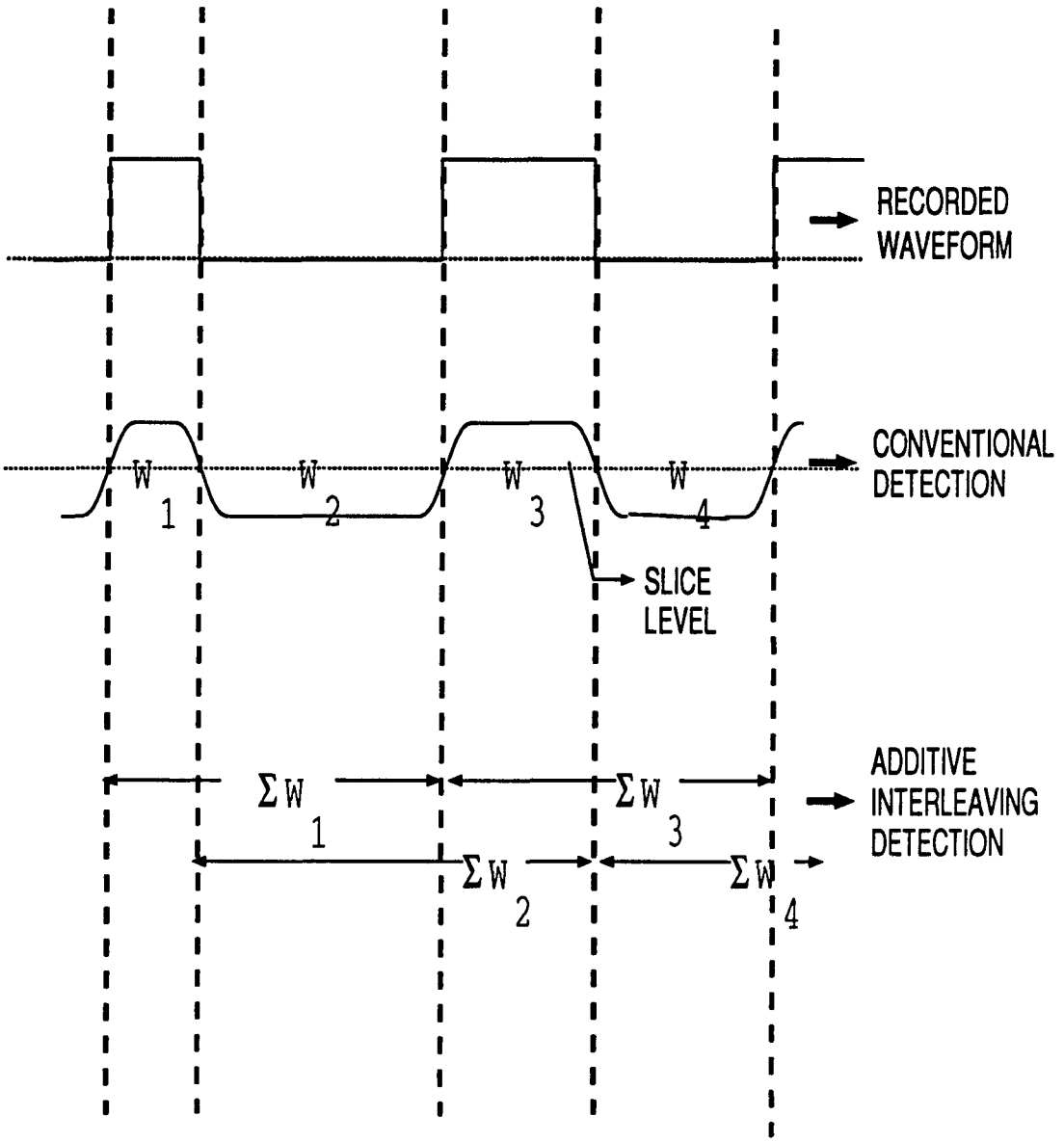

Figure 5.3: Additive Interleaving Detection.

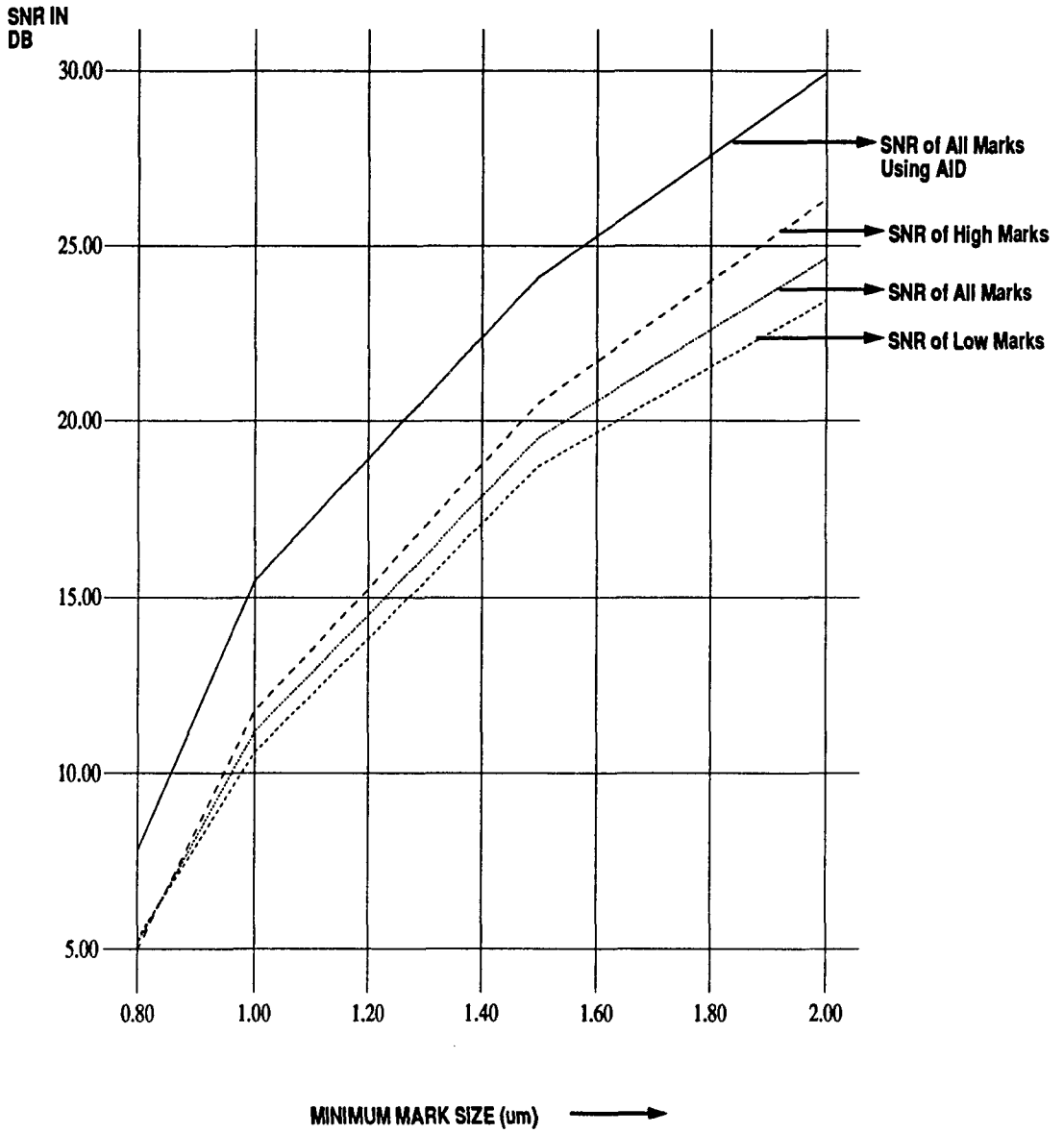

Figure 5.4: SNR of Pseudorandom Sequence Without Equalization.

(3 to 5 dB better). From Fig. 5.5, we also see that equalization can improve SNR significantly and even better than the case using AID detection (0 to 3 dB better).

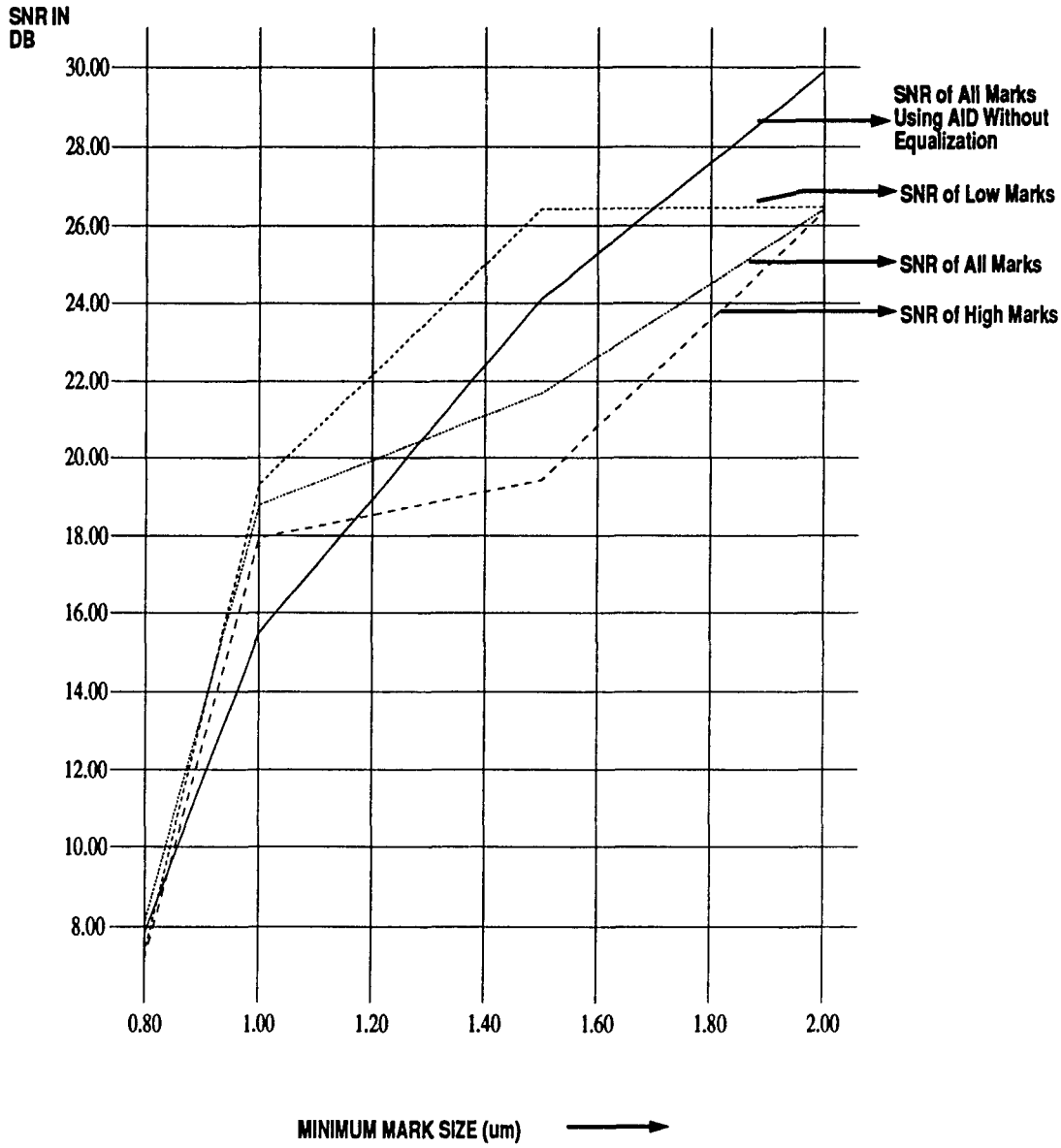

Figure 5.5: SNR of Pseudorandom Sequence With Equalization.

CHAPTER 6

Discussion and Conclusion

From the experimental results, following observations are made:

1. The ISI characteristics in optical data storage systems are highly non-linear in nature. The empirical relation given by Eq. (4.5) closely matches the actual ISI characteristics.

2. The method of digitizing the readback signal and determining mark sizes using signal processing techniques is highly successful as it gives very consistent results.

3. The SNR obtained using Additive Interleaving Detection (AID) is much better than SNR without equalization. This better performance from AID can be understood by noting that in M-O systems, high marks and low marks have correlated ISI characteristics. By measuring two marks together, much of the ISI effects from the two can be canceled.

4. SNR can be improved significantly by equalization process utilizing the empirical relation given by Eq. (4.5).

This thesis discussed the ISI characteristics for a Nakamichi M-O data storage system and studied how SNR can be improved by using ISI equalization and AID detection. The

approach of digitizing the read back signal was very successful and AID was much better than simple detection without equalization.

The goal in the future is to use the current ISI model and equalization techniques to improve higher storage densities with more advance coding and detection techniques. We would like to extend our ISI model and equalization techniques to coding schemes such as Partial Response codes. In this thesis we obtained ISI characteristics at constant linear velocity. If the disk rotates at constant angular velocity then ISI will vary with track radius. We would like to determine this variation of ISI with track radius. We would also like to determine how ISI characteristics vary with laser power variation during the read/write process. A better understanding of other noise sources like material defects, laser beam fluctuation, etc also needs to be done.

APPENDIX A

In this appendix we describe the algorithm used for smoothing the digitized waveform. Let y_i be the amplitude of the i^{th} data point of the raw waveform and $\hat{y}_i$ be the amplitude of the i^{th} data point of the smoothed waveform.

$\hat{y}_i$ is determined by taking 5 data points before and 5 data points after the i^{th} data point. $\hat{y}_i$ is estimated as

$$\hat{y}_{i+k} = a_2 x_{i+k}^2 + a_1 x_{i+k} + a_0 \tag{A.1}$$

$$= \sum_{j=0}^{2} a_j x_{i+k}^j \tag{A.2}$$

where $k = 0, \pm 1, \ldots, \pm 5$, and x_i is the time point corresponding to y_i shifted by i positions. Therefore, we simply set $x_i = 0$ The coefficients a_j are determined as follows:

Let z be the square sum of differences between y_{i+k} and $\hat{y}_{i+k}$ for $k = 0, \pm 1, \ldots, \pm 5$. We then have

$$z = \sum_{k=-5}^{5} (y_{i+k} - \hat{y}_{i+k})^2 \tag{A.3}$$

$$= \sum_{k=-5}^{5} (y_{i+k} - \sum_{j=0}^{2} a_j x_{i+k}^j)^2. \tag{A.4}$$

To Minimize z with respect to each of a_j, we set

$$\partial z / \partial a_j = -2 \sum_{k=-5}^{5} (y_{i+k} - \sum_{j=0}^{2} a_j x_{i+k}^j) x_{i+k}^j \tag{A.5}$$

$$= 0. \tag{A.6}$$

The above expression yields the 3 following equations:

$$\sum_{k=-5}^{5} y_{i+k}x_{i+k}^2 = \sum_{k=-5}^{5} a_2x_{i+k}^4 + \sum_{k=-5}^{5} a_1x_{i+k}^3 + \sum_{k=-5}^{5} a_0x_{i+k}^2 \quad \text{(A.7)}$$

$$\sum_{k=-5}^{5} y_{i+k}x_{i+k} = \sum_{k=-5}^{5} a_2x_{i+k}^3 + \sum_{k=-5}^{5} a_1x_{i+k}^2 + \sum_{k=-5}^{5} a_0x_{i+k} \quad \text{(A.8)}$$

$$\sum_{k=-5}^{5} y_{i+k} = \sum_{k=-5}^{5} a_2x_{i+k}^2 + \sum_{k=-5}^{5} a_1x_{i+k} + \sum_{k=-5}^{5} a_0. \quad \text{(A.9)}$$

Eqs. (A.7), (A.8) and (A.9) expressed in matrix form gives

$$\begin{pmatrix} \sum_{k=-5}^{5} x_{i+k}^4 & \sum_{k=-5}^{5} x_{i+k}^3 & \sum_{k=-5}^{5} x_{i+k}^2 \\ \sum_{k=-5}^{5} x_{i+k}^3 & \sum_{k=-5}^{5} x_{i+k}^2 & \sum_{k=-5}^{5} x_{i+k} \\ \sum_{k=-5}^{5} x_{i+k}^2 & \sum_{k=-5}^{5} x_{i+k} & \sum_{k=-5}^{5} \end{pmatrix} \begin{pmatrix} a_2 \\ a_1 \\ a_0 \end{pmatrix} = \begin{pmatrix} \sum_{k=-5}^{5} y_{i+k}x_{i+k}^2 \\ \sum_{k=-5}^{5} y_{i+k}x_{i+k} \\ \sum_{k=-5}^{5} y_{i+k} \end{pmatrix}.$$

The above set of equations are solved for each data point to get a new set of values which represent the smoothed waveform.

REFERENCES

[1] R. L. Adler, D. Coppersmith and M. Hassner, "Algorithms for sliding block codes," *IEEE Trans. Inform. Th*, vol. H-29, Jan. 1983.

[2] J. H. Cioffi, W. L. Abbott, H. K. Thapar, C. M. Melas and K. D. Fisher, " Adaptive equlization in magnetic-disk storage channels," *IEEE Commun. Magazine*, Feb. 1990.

[3] E. D. Daniel and C. D. Mee, *Magnetic Recording Handbook.* McGraw-Hill, 1989.

[4] G. D. Forney, Jr., "Maximum-likelihood sequence estimation of digital sequences in the presence of intersymbol interference," *IEEE Trans. Inform. Theory*, vol. IT-18, pp. 363-378, May 1972.

[5] J. W. Goodman, *International Trends In Optics.* Academic Press Limited, 1991.

[6] S. Haykin, *Adaptive Filter Theory.* Prentice-Hall, Englewood Cliffs, N.J., 1986.

[7] Hewlett Packard Application Note 358-3, "Time domain characterization of magnetic disk drives".

[8] D. G. Howe, "Signal-to-noise ratio (SNR) for reliable data recording," SPIE vol. 695 - Optical Mass Data Storage II, 1986.

[9] D. G. Howe, "The nature of intrinsic error rates in high density digital optical recording," SPIE vol. 421 - Optical Disks Systems and Applications, 1983.

[10] E. A. Lee and D. G. Messerschmitt, *Digital Communication.* KAP, Boston, 1988.

[11] M. M.-K. Liu, "Jitter Model and Signal Processing Techniques for High-Density Optical Data Storage," *IEEE Journal on Selected Areas in Communications*, vol. 10, No. 1, Jan. 1992.

[12] M. M.-K. Liu, S. Gupta and B. Tehranchi, "Intersymbol Interference Characterization and Equalization for High-Density Optical Data Storage" *Submitted to IEEE Global Telecommunications Conference*, March 1992.

[13] M. M.-K. Liu, "Experiments for future high density optical data storage," paper presented in Optical Data Storage meeting, University of Arizona, Tucson, Apr. 1990.

[14] T. Maeda, A. Saitoo, H. sugiyama, M. Ojima, S. Arai and K. Shigematu - Hitachi Ltd., "High speed large capacity optical disk using pit-edge recording and MCAV method".

[15] M. Mansuripur and G. A. N. Connell, "Signal and noise in magneto-optical readout," J. Appl. Phys. 53(6), June 1982.

[16] Nakamichi U.S.A. Corp., *Optical Memory System - 1000* Nakamichi U.S.A. Corp.

[17] J. G. Proakis, *Digital Communications.* McGraw-Hill, 1989.

[18] H. Sukeda, H. Tsuchinaga, S. Tanaka, T. Niihava, S. Nakamura and S. Mitra - Hitachi Ltd., Y. Yamada and N. Ohta - Hitachi Maxell Ltd. and M. Fukushima - Nippon Columbia Co. Ltd., "High speed recording technologies for magneto-optical disk system".

[19] R. W. Wood and D. A. Petersen, "Viterbi detection of class IV partial response on a magnetic recording channel," *IEEE Trans. Commun.*, vol. COM-34, pp. 454-461, May 1986.